Light charged particle and neutron velocity spectra in coincidence with projectile fragments in the reaction ^{40}Ar(44 A.MeV)+^{27}Al *

G. Lanzanò, E. De Filippo, M. Geraci, A. Pagano

S. Aiello, A. Cunsolo, R. Fonte, A. Foti, M.L. Sperduto

Istituto Naz. Fisica Nucleare and Dipartimento di Fisica

Corso Italia 57, 95129 Catania, Italy

C. Volant, J.L. Charvet, R. Dayras, R. Legrain

DAPNIA/SPhN, CEA/Saclay, 91191 Gif-sur-Yvette Cedex, France

(July 26, 2000)

Abstract

We present a three source analysis of velocity spectra of light charged particles (LCP) and neutrons emitted in the reaction ^{40}Ar+^{27}Al at 44 A.MeV. The light particle (LP) velocity spectra are studied as a function of the detection angle ($1.5°<\theta<172°$) and of the charge of the forward detected projectile-like fragment (PLF). The temperature parameter, the velocity and the intensity of each source are extracted as a function of the PLF charge. While the temperature parameters for PLF and target-like fragments (TLF) are very similar and show a dependence on the PLF charge, the temperature parameter for the intermediate source is approximately 15 MeV, independent of the PLF charge. Comparison with temperature values extracted from double isotopic ratios, shows an agreement only between the temperature values extracted

*Experiment performed at GANIL.

from formula involving ^{3}He, ^{4}He, d, t ratios and the PLF proton temperature parameter. The characteristics of the PLF sources are derived. Present results are discussed with regards to the degree of thermalization which could be achieved in the PLF and TLF sources.

Keywords: Intermediate energy, ^{40}Ar+^{27}Al reaction, E=44 A.MeV, projectile-like fragment, light particle, coincidence, temperature, emitting source.

PACS: 25.70.Pq, 25.70.Mn

I. INTRODUCTION

It is widely known that the study of light particles and light fragments emitted in heavy ion nuclear reactions can give some insight on the involved reaction mechanisms. This is certainly true at low energies where, following fusion, simple spectra, characteristic of the formed compound nucleus, are found. By increasing the bombarding energy, although the binary nature of the collision dominates, the experimental particle energy spectra become more complex, suggesting either that an important part of the particles are dynamically emitted before a thermo-dynamical equilibrium is reached or/and that more than one or two emitting sources are present. The main information relative to their emission or to the properties of the emitting sources, can be extracted from the shape of energy spectra, angular distributions, multiplicity and their relative abundances [1–4].

In the past some emphasis has been put on an intermediate velocity source in studying these spectra [1,2]. This has led, for instance, to study LCP inclusive energy spectra at a few selected intermediate laboratory angles. However, it was clear since the first experiments at intermediate energies that at least two other main sources were present, of which one with a velocity close to the beam velocity and the other with a velocity close to the target velocity. Then the idea of unfolding the complex LP spectra in at least three components can appear natural and for some aspects necessary for a comprehension of the scenario involved in the

reaction mechanism. In this context a three source study has been recently carried out either on LCP exclusive velocity [5,6] and inclusive energy [7] spectra in a large angular range, for the reaction ^{40}Ar+^{27}Al respectively at 44 and 60 A.MeV. Many other experimental efforts have been devoted in the last years to characterize the various emission processes in different intermediate energy heavy ion collisions [8–17]. Recently also, accurate Landau-Vlasov calculations [18] have been carried out: the authors show evidences for dynamical effects of particle emission in binary dissipative collisions; in particular they study the consequences on the nucleus heating and the possible formation of an intermediate source.

In the following we present the results of an exclusive experiment performed at GANIL using the multidetector ARGOS. The aim of the experiment was to get a comprehensive view on the reaction scenario, by detecting as many reaction products as possible and by using different targets. The main peculiarities of the present experiment are the following.

I) LP and PLF velocity spectra are directly and accurately measured by means of Time-of-Flight (ToF) technique.

II) The involved detection angular range is very large. LP velocity spectra have been measured at 24 laboratory angles, between 1.5° and 172°.

III) LP velocity spectra are measured in this angular range in coincidence with projectile-like-fragments (PLF) detected in a large forward solid angle, between 0.75° and 7°. PLF-PLF coincidences in the forward wall have also been recorded and will be the argument of a separate paper.

As it will be stressed in the paper, the analysis of the LP spectra has been accomplished by assuming that the particles are emitted from three equilibrated moving sources, described by two maxwellian energy distributions with surface emission and one assuming volume emission, respectively for the two sources with velocities close to the projectile and target ones, and for the source with velocity intermediate between them. The reliability of the extracted parameters lies in the fact that the "evolution" of LP velocity spectra from forward to backward direction in the laboratory frame is "followed" continuously by small angular steps, so that some ambiguities arising in the fit procedure are strongly reduced, by imposing

that the agreement between experimental spectra and theoretical calculations is equally good in the whole angular range.

After a brief description of the experimental set-up, we shall present the method used in the data analysis and the results for the LP-PLF coincidences.

II. EXPERIMENTAL LAYOUT

The experiment has been performed at GANIL, by bombarding a 200 μg/cm^2 thick self-supporting ^{27}Al target with a 44 A.MeV ^{40}Ar pulsed beam. The nuclear products issued from the reaction were detected by means of ARGOS, a multidetector made by 112 separate hexagonal BaF_2 crystals, modified into phoswichs, by means of a fast plastic scintillator sheet, of suitable thickness, according to the charge and dynamical range of the ion to be detected [19–21]. Each crystal has a surface of 25 cm^2 and a variable thickness up to 10 cm, stopping protons of energy up to 200 MeV.

In the present experiment the ARGOS multidetector was placed in the Nautilus scattering chamber at GANIL, with the following geometry (see Fig. 1). A forward wall of 60 phoswichs was placed between 0.7° and 7° in an honeycomb shape at a distance of 233 cm from the target (solid angle: 0.03 sr); they detected PLF identified in charge and LCP isotopically separated. The angular separation between the centers of two adjacent detectors was $\approx$ 1.5°.

A backward wall of 18 phoswichs was placed between 160° and 175° at a distance of 50 cm from the target (solid angle: 0.2 sr), for the detection of LCP and neutrons.

A battery of 30 phoswichs was placed in a plane on both sides of the beam at a distance from the target ranging from 0.5 m to 2 m following the expected counting rate, between 10° and 150°.

In this experiment we used plastic scintillator thicknesses of 700 and 30 μm for the forward wall and the remaining detectors respectively.

Shape discrimination of the photomultiplier signals and time-of-flight techniques [22]

have been exploited for a full identification of all the reaction products, including neutrons. For neutrons, the efficiency depends mainly on the crystal thickness and on the electronic threshold [23,24]. Typically, neutron efficiency values of about 8% are observed for 5 cm thick crystals and 1 MeV electron equivalent threshold [24].

For all detected particles the calibration was done by time-of-flight measurements, gamma-rays giving a reference time for the in-plane detectors and in the backward wall, whereas elastically scattered particles were used for the detectors placed in the forward wall. Time resolutions between the cyclotron RF and the photomutipliers were typically 400-600 ps, depending on the detectors and runs and never exceeded 1 ns.

Events were recorded each time the in-plane detectors or the backward wall triggered, a minimum total multiplicity of 2 being requested.

III. ANALYSIS OF THE LIGHT PARTICLE VELOCITY SPECTRA

Fig. 2 shows a typical bidimensional plot of the invariant cross-section, for α-particles in coincidence with Z=16 PLF detected in the forward wall. To construct such bidimensional plots we have calculated from the experimental data the invariant cross-section as $\sigma_{inv} = \frac{1}{2\pi v_\perp}\frac{d^2\sigma}{dv_\parallel dv_\perp}$ at each detector angular position. In the forward direction the angular interval was 5° up to 50° and thereafter ≈10° up to 175°. This allowed us to interpolate between two adjacent angles to obtain "continuous" invariant cross-section bidimensional plots like the one reported. Experimental thresholds are between 1 and 2 cm/ns. Two sources are clearly visible, the velocities of which are very close respectively to the initial velocities of the projectile (8.9 cm/ns) and of the target. However some particles with velocity intermediate between these two are also present in the plot, suggesting the occurrence of dynamically emitted particles from the overlap zone of the two interacting nuclei, that can be thought as a third source of particles. The pattern of the bidimensional plot of the invariant cross-section, like the one shown in Fig. 2, depends on the coincident PLF atomic number as it is evident from Fig. 3 for the PLF-proton coincidences. In fact when the PLF atomic

number decreases the LP sources become less and less evident. In addition we observe an increasing coincidence rate between light heavy ions, with a charge correlation peaked near Z=6, suggesting a more complex decay mechanism for the excited projectile, like fission or cracking [25]. This projectile break-up accounts for the anomalously high yield near carbon as already observed in inclusive PLF mass and charge distributions [26]. The study of these PLF-PLF coincidences [6] will be presented in a separate paper. For PLF of charge ≥ 9 the two sources are well separated. Their centroids show also a slight dependence on the PLF atomic number, as already observed in inclusive experiments [26].

With the assumption that the LP are emitted by three independent moving equilibrated sources, we have fitted simultaneously for one particle type and one given PLF all the velocity spectra from 1.5° to 175° assuming maxwellian energy distributions. More precisely we assume a surface emission for the two sources with velocities close to the projectile (PLF source) and target (TLF source) ones and a volume emission [27,28] for the source with a velocity intermediate between them (INT source), more reminescent of a fireball. Fits obtained by substituting the two surface-maxwellians by two volume-maxwellians, give a worse agreement especially at the most forward angles, where the forward-backward emission was not reproduced.

In the source frame of reference, surface emission (TLF and PLF sources) obeys the relation,

$$\left(\frac{d^2N}{d\Omega dE}\right)_{cm}^{surf} = A_1(E_{cm} - B_c)e^{-\frac{(E_{cm}-B_c)}{T}} \qquad (1a)$$

whereas volume emission (intermediate velocity source) is governed by,

$$\left(\frac{d^2N}{d\Omega dE}\right)_{cm}^{vol} = A_2\sqrt{(E_{cm} - B_c)}e^{-\frac{(E_{cm}-B_c)}{T}} \qquad (1b)$$

where E_{cm} is the kinetic energy of the particle, B_c the Coulomb barrier and T the temperature of the source.

By transforming to the laboratory system and by taking as appropriate variable velocity

instead of energy, we have for $v_{cm} \geq v_c$, with $v_c = \sqrt{2B_c/m}$:

$$\left(\frac{d^2N}{dvd\Omega}\right)_L^{surf} = N_i\left(\frac{m^2}{8\pi c^4 T^2}\right)\frac{v_L^2(v_L^2+v_S^2-2v_Lv_Scos\theta-v_c^2)}{\sqrt{v_L^2+v_S^2-2v_Lv_Scos\theta}}\times$$
$$\times e^{-\frac{m}{2c^2T}(v_L^2+v_S^2-2v_Lv_Scos\theta-v_c^2)} \qquad (2a)$$

$$\left(\frac{d^2N}{dvd\Omega}\right)_L^{vol} = N_i\left(\frac{m}{2\pi c^2 T}\right)^{\frac{3}{2}}v_L^2\sqrt{\frac{v_L^2+v_S^2-2v_Lv_Scos\theta-v_c^2}{v_L^2+v_S^2-2v_Lv_Scos\theta}}\times$$
$$\times e^{-\frac{m}{2c^2T}(v_L^2+v_S^2-2v_Lv_Scos\theta-v_c^2)} \qquad (2b)$$

where v_L and θ are respectively the velocity and the emission angle of the particle in the laboratory, c is the velocity of light and v_S the source velocity. N_i are normalisation factors.

The total velocity distribution is then given by the following function:

$$\left(\frac{d^2N}{dvd\Omega}\right)_L = \left(\frac{d^2N}{dvd\Omega}\right)_{L,PLF}^{surf} + \left(\frac{d^2N}{dvd\Omega}\right)_{L,TLF}^{surf} + \left(\frac{d^2N}{dvd\Omega}\right)_{L,INT}^{vol} \qquad (2c)$$

Let us comment on the different behaviour of formulae 2a) and 2b). At the most forward angles, in particular at θ=0°, and for v_c=0 they reduce to:

$$\left(\frac{d^2N}{dvd\Omega}\right)_L^{surf} = N_o\left(\frac{m^2}{8\pi c^4 T^2}\right)v_L^2|v_L-v_S| \times e^{-\frac{m}{2c^2T}(v_L-v_S)^2} \qquad (3a)$$

$$\left(\frac{d^2N}{dvd\Omega}\right)_L^{vol} = N_o\left(\frac{m}{2\pi c^2 T}\right)^{\frac{3}{2}}v_L^2 \times e^{-\frac{m}{2c^2T}(v_L-v_S)^2} \qquad (3b)$$

Thus in the case of neutrons and a source velocity v_s=8 cm/ns, while formula 2a) (surface emission) predicts a double humped distribution, that accounts for forward and backward emission, formula 2b) (volume emission) does not (see Fig. 4). This effect is due to the kinematics since indeed, in the lower part of Fig. 4, it is shown that the velocity distributions in the emitter frame are quite similar using both formulas. For charged particles, due to Coulomb effects, the two formula results are only slightly different at the most forward angles. At largest angles, these differences are vanishing because of kinematical effects.

For each source, N, v_s, T and v_c were treated as free parameters. In a first step, for a given particle and a given PLF, assuming three independent moving sources, the corresponding twelve parameters were determined by a simultaneous χ^2 fit to all velocity spectra from 1.5° to 172°. In fact, these preliminary calculations gave us the following indications concerning the intermediate source: the obtained values for v_s and v_c fluctuated around $v_P/2$ and 0 respectively as a function of the PLF charge. Then, in order to overcome the problem of coupling between the parameters, we decided to fix these parameters to the constant values $v_P/2$ and 0 respectively.

In the case of the PLF source, the v_c parameter was very sensitive to the PLF charge. This was not the case for the TLF source, where only a slight dependence was observed around a mean value. This fact can be understood if we admit that a given projectile-like fragment is in coincidence with a rather broad target-like fragment distribution, as already observed [29]. However, this mean value, that we have fixed to v_c=1 cm/ns for all PLF charges in the present case of Al target, is very sensitive to the target nature.

Data obtained in the same experiment on various targets at the most backward angle, 172°, where the influence of the target is expected to be stronger show that the maximum of the velocity spectra shifts towards higher velocity values, while the slope of the spectra remains practically unchanged, when going from carbon to thorium [5].

For ^3He particles the statistics was scarce and it was difficult to separate them from tritons and α-particles. Therefore it was decided to fit ^3He particle spectra using the same parameters as for the tritons except for the normalisation coefficients which were kept free. Considerable uncertainties can affect the extracted neutron yield. They are associated in part with the estimated values of the BaF_2 efficiency to neutrons, and in part with cross-talk effects, more important in the forward direction, where the majority of the detectors are concentrated.

For a given PLF, several attempts were made to obtain a single set of parameters for all the particles, without success. We have then applied this fit procedure for each particle species and for each PLF charge. The quality of the fits is illustrated in Fig. 5-7. Emission by

an equilibrated excited projectile or PLF is evident at the most forward angles and is fairly well reproduced by the calculations. Similarly, the emission at the most backward angles is completely dominated by an equilibrated excited target or TLF. Finally the intermediate source dominates at angles close to 40°, as already observed in an inclusive experiment [7]. For the most forward LP angles (see Fig. 7) and specially for PLF charges close to the one of the projectile, the calculation systematically overestimates the experimental points at velocities around the half of the beam velocity. This could lead to an overestimation of the intermediate source intensity in this angular range. However the global contribution of this component is mainly fixed by the intermediate angular domain.

From this fit procedure we have extracted source velocities, temperatures and intensities. We have extended the analysis from Z_{PLF}=19 down to Z_{PLF}=7, even if below Z_{PLF}=9 the signature of the two sources is not so evident, as stressed above. Fig. 8 shows the velocity for PLF and TLF sources, as a function the PLF charge for different LP species. As expected [26,29], for decreasing PLF charge, the PLF source velocity is decreasing, while the velocity of the TLF source is increasing. A very slight dependence on the light particle type is seen. In fact, for a given PLF charge, we observe that the PLF source velocity is higher for neutrons and lower for more complex particles like deuterons and tritons. The contrary is observed in the case of the TLF source.

For the PLF source, the Coulomb parameter B_c is linearly increasing with the PLF charge and shows a marked dependence on the particle species (see Fig. 9).

Fig. 10 (symbols) reports the temperature parameter T of the three sources as a function of the PLF charge and the particle species. Starting from the projectile charge, the temperature of both PLF and TLF sources slightly increases as the PLF charge decreases until a plateau is reached at around 5-7 MeV for Z$\leq$9. The temperatures found for these two sources are almost the same and a noticeable dependence upon the particle type is observed. The lowest temperatures are associated to neutrons whereas the highest ones are associated to tritons. For the intermediate source, if we except the anomalous behavior of α-particles with a decreasing temperature from T=15 MeV (Z=19) to T=10 MeV (Z=9), we find an

almost constant temperature of about 14-16 MeV for all the other particles as a function of the PLF charge, as already found in previous inclusive experiments [2]. Note that, since in the present procedure the recoils are not taken into account, B_c and T values might be underestimated especially for the lowest Z_{PLF} values.

Fig. 11 shows the different LP multiplicity in the three sources as a function of PLF charge detected in the forward wall. For the three sources and for $Z_{PLF} \geq 12$, the multiplicities are increasing when Z_{PLF} decreases, thus giving an indication of the link between the PLF charge and the violence of the collision. However one observes also a multiplicity saturation for the lowest Z_{PLF} values. One notes that α-particles are as much abundant as protons. One can also notice that the neutron rich LCP (deuterons ant tritons) are more abundant in the intermediate source than in the two other ones. The light particle multiplicity of this source is comparable to the PLF and TLF source ones. Neutron multiplicities are larger than proton ones for the intermediate source, and almost equal for the TLF source. Since cross-talk effects in the forward wall can heavily affect the neutron yield, no neutron multiplicities have been reported for the PLF source. Anyway this neutron emission for the PLF source (after correction for detector efficiency and estimate of cross-talk contribution) appears to be important, this could be probably connected with the particular nature of the projectile, a neutron-rich nucleus.

The main results of the fit analysis (parameters and LP contributions for the three sources) are summarized in Table I.

IV. DISCUSSIONS

In the light of these results, we want to discuss some topics of recent interest.

A. Temperatures from isotopic ratios

First of all, if the sources are well separated, following [7] we can combine in a proper way the results of table I in order to obtain temperatures by computing the isotopic ratios,

as suggested in [30]. The results are summarized in table II, in which the temperatures are reported for the three formulas of reference [7], dα-t^{3}He, dd-pt and pα-d^{3}He, respectively T_1, T_2 and T_3 in table II, for each source and for each PLF charge. We observe that the results given by the three formulas are in general different, the first and third ones agree better between themselves. Furthermore and unexpectedly the T_2 temperature for the PLF source decreases with decreasing Z_{PLF}. In the following we concentrate ourselves on the results of the first formula. By comparing now the results of tables I and II, we find the largest discrepancy for the intermediate source, an average of 15 MeV for the temperature parameter and an average of 4 MeV from the isotopic ratios. For PLF and TLF sources we find the best agreement between the T_1 temperatures and the temperature parameters as obtained from proton spectra. The meaning of this agreement is not clear and we can also notice that proton contribution is not taken explicitely into account in T_1. Furthermore the discrepancy for the intermediate source is unexpected since the formalism of ref. [30] would be more appropriate to describe a low density gaseous matter which one can believe to be reached in this source. The results of isotopic ratio calculations are illustrated by curves in Fig. 10.

B. Neutrons

Although the neutron detection can be affected by several important sources of errors, we observe however that PLF neutrons present the lowest temperature parameters, $\approx$1 MeV lower than the one relative to protons. This could be due to the difficult efficiency corrections as a function of energy [23,31] since neutron and proton energy spectra are found compatible in other experiments [32]. Further works are in progress to clarify this point. The fact that the ^{40}Ar projectile is neutron-rich could explain the observed large abundance of PLF neutrons. If we suppose that on the average each PLF is accompanied by 2-3 neutrons, as supported by evaporative calculations, the large neutron cross-sections mentioned above can be easily understood. On the contrary, TLF neutron numbers are lower in agreement

with the different nature of the target.

C. Excitation energies and caloric curve

Recently much effort has been done, also by means of 4π detectors, to construct a relation between temperature and excitation energy of a nuclear system (the so-called caloric curve), mainly to put in evidence a possible "phase-transition" in nuclear systems [33–38]. Up to now no unambiguous solution has been given to this problem. The difficulty resides in the applicability of the thermal concepts to nuclei. Even when this hypothesis is admitted, how accurately can we measure independently excitation energies and temperatures ? Besides the manner to get rid of the dynamical effects, no need to cite also the different choices of thermometers (isotopic ratios, slopes of energy spectra, relative population of unstable states, etc..). They give different results and the explanation given is that they are sensitive to different time stages in the hot nuclei decay. Here, we used two thermometers. The first one, the isotopic ratio method, gives different measurements depending on the chosen ratio. We will consider in the following the results of the second method, using fits to the velocity spectra, to examine which contribution our data can give to this topic.

In our experiment we have no direct access to the excitation energies involved in the different sources. However we will try to determine them by assuming that our temperature parameters T (Table I) have a physical meaning at least for the PLF and TLF sources. We will concentrate on the PLF source using a method similar to the one described in [17]. A reconstruction of the mean primary charge PLF source Z^*_{PLF} is done by using the multiplicities $< mult_i >$ of LCP of charge Z_i from the top of Fig. 11 and including the charge of the PLF.

$$Z^*_{PLF} = \Sigma_i < mult_i > \times Z_i + Z_{PLF} \qquad (4)$$

An estimation of the involved mean excitation energy $< E^*_{PLF} >$, has been made by means of a calorimetric method, which takes into account the multiplicities $< mult_i >$ (from Fig. 11), barrier energies B_c (from Fig. 9) and temperatures T_i (see Fig. 10 and Table I).

The primary mass M^*_{PLF} is deduced from Z^*_{PLF} assuming the same neutron/proton ratio as in the projectile.

$$< E^*_{PLF} >= \Sigma_i < mult_i > \times (m_i c^2 + < E_i >) \; - \; M^*_{PLF} c^2 \qquad (5)$$

where m_i's are the masses and $< E_i >= 2. \times T_i + B^i_c$ are the average LP kinetic energies. The neutron multiplicities are deduced from mass conservation.

The results are reported in Fig. 12a) for the primary PLF charges. Taking into consideration the presence of an intermediate source, makes the primary PLF charge go away from the projectile charge as the detected PLF charge decreases. Our data are in excellent agreement with the predictions of [18] (the squares in Fig. 12 a)). For sake of comparison, in the same figure is reported the predicted mean primary PLF charge as obtained by means of an abrasion-ablation calculation [26,39,40]. The disagreement, also observed in [17], is probably due to the fact that the primary PLF properties are obtained only from geometrical considerations. A better agreement may be achieved by using more recent versions of the abrasion model, that take explicitely into account different and more realistic mechanisms to build the primary PLF [41–43].

The deduced excitation energies for the PLF sources are shown in Fig. 12b) as a function of the PLF charge. We report also for the same system the predictions of two extreme models: a geometric abrasion model [26,39,40] and the results of [29] obtained by supposing that a binary reaction mechanism was responsible for the observed PLF-TLF correlations. To plot the last relation (stars in Fig. 12b)), the detected PLF masses in [29] have been converted in PLF charges assuming the same neutron/proton ratio as in the projectile. The experimental points lie in between the predictions of these two extreme reaction mechanisms.

Finally Fig. 12c) shows the PLF caloric curves deduced by using two different thermometers. The PLF excitation energies are those obtained from the previously described calorimetry method and the temperature parameters for protons and α-particles are extracted from Table I. We want to stress at this point two facts. First, excitation energies are limited to 3-4 A.MeV; that corresponds to temperatures of 4-5 MeV. These values could be compared to apparent emission temperatures deduced from the relative population of states

in ^{5}Li, showing a flattening in the temperature distribution at around 3.5-4.5 MeV [44]. The fact that the PLF and TLF source light particle multiplicities tend to saturate or decrease for PLF charge lower than 9, (Fig. 10) could corroborate this limitation but a delicate interplay between the increase of the excitation energies and the decrease of the primary PLF masses could also explain this observation. A decrease of the PLF charge or equivalently of the impact parameter, would contribute essentially to increase the intermediate source light particle emission, as found in [16,18]. Secondly, as already shown in Fig. 10, the temperature parameters associated with these excitation energies do depend on the particle species. This fact, already observed in other analysis [7], needs further considerations.

Notice that the experimental determination of these caloric curves depends on how much accurate is the determination, from our data, of the temperatures and, independently, of the associated excitation energies. For temperature estimates we feel that the use of the full measurement results, i.e. the yields and shapes of the particle spectra, permit to keep more information than when reducing the data to isotopic ratios. We can also point out that the experimental excitation energies of Fig. 12c) would have shifted towards higher values (around 5-6 A.MeV) if a binary mechanism was supposed. Besides the needed demonstration that a thermal equilibrium is reached, the proposed caloric curves must be considered with some caution.

D. Intermediate source

Finally, let us discuss some results concerning the intermediate source. There is no direct experimental evidence for this source by looking at invariant plots of the type as in Fig. 2. Therefore a better characterization of this source can be made only by a "subtraction" method, knowing in a complete and fine way the properties of the other two, PLF and TLF, sources. In fact, particles of different origins (distinct from PLF and TLF sources) may come together into this source, like prompt particles emitted in the very first stage of the reaction or particles dynamically emitted from the interaction zone. In this context our

parameterization of the intermediate source could be thought inadequate, but it must be regarded as the best "equilibrium source" able to simulate the properties of these particles centered at intermediate velocities. However, the relative importance of this source has a physical significance and can be compared, for instance, to the predictions of recent dynamical Landau-Vlasov calculations of ref. [18], for protons emission from the same system at 65 A.MeV. Following the results of Table I relative to protons and to the intermediate source, we find a slight increase of the intermediate source intensity as the PLF charge decreases from Z_{PLF}= 19 to 9 with an average value of $\approx$0.28, relatively to the sum of the three contributions. This trend is in a fair agreement with the predictions of Fig. 3 of ref. [18], from which, however, a higher mean value of $\approx$0.47 can be deduced for peripheral impact parameters between 3.5 and 6.5 fm, corresponding to PLF masses between 23 and 40 [40]. Part of the discrepancy could be attributed to the different bombarding energies. Despite the fair agreement, we must remind that this model is very simplistic and restrictive, inasmuch only protons and neutrons are predicted as particles issued from the interaction zone. For instance, no comparison can be made with the relative production of composite particles.

The relative contributions of each source are reported in Fig. 13 for each particle as a function of the PLF charge. Only for protons we report also the predictions of [18] for the INT source. The theoretical calculations show a qualitative agreement with the data: the trend of the relative contribution variation with the PLF charge is reasonably accounted for as well as the magnitudes.

For the most peripheral collisions, the main α-particle yield is due to the TLF. This relative yield decreases with the decrease of Z_{PLF}, this trend is opposite for the PLF source. In fact, the selection of large Z_{PLF} values implies low excitation energies in the PLF source but the coincident TLF sources can exhibit a larger dispersion in masses, charges and excitation energies [45] and hence can induce such an effect which is visible for all LP in the peripheral region.

One can also notice in Fig. 13 that the major production of deuterons and tritons is due to the intermediate source as seen also in [16]. This could explain why these particles

exhibit, in the PLF and TLF sources, a temperature on the average higher than for protons and neutrons: in other words, the PLF and TLF sources can be "contaminated" by the presence of the much more intense intermediate source. In fact a large overlap between this source and the others in the velocity space is theoretically predicted [18] and found in recent analysis [17,45]. It is hence difficult to disentangle the various components. In Fig. 13, one also observes that, for the INT source, the relative yields for deuterons and tritons decrease with Z_{PLF} in contrast to protons and α-particles. These behaviors with the variation of centrality need further investigations; unfortunately the theoretical results cannot yet be confronted with this finding. Part of the explanation could be that in peripheral reactions (large Z_{PLF}), the overlap zone keeps memory of the neutron richness of the projectile.

The temperature parameter of the intermediate source is abnormally high, exceeding the available energy. Its location in the invariant plots in Fig. 2 and 3 does not show up, although it could be masked by the spheres of emission from TLF and PLF. Further, the mean transverse energies of these intermediate velocity particles are found particularly high [16,17] which is incompatible with an equilibrated emission from the PLF and TLF but which is also in agreement with our high temperature parameter. These facts throw some doubts on its achieved thermal equilibrium and meaning. As stressed in [18], an interpretation in terms of prompt particles emitted in the first stage of the interaction is a more suitable explanation for this intermediate source, and, let us say, is more appropriate in this incident energy range. Further also, present developements tend to explain part of this intermediate component as prompt emissions following nucleon-nucleon collisions in the overlap region of the two colliding partners [46].

The presence of this component has the consequence that the claim of formation of very hot equilibrated nuclei in this domain of energy has to be taken with great care [36,47]. The temperature extracted from the velocity spectra of neutrons, the most abundant particles in the PLF source, could be a cleaner physical observable to derive the PLF system temperature. This deserves much more attention from experimentalists in this energy domain [4,13]. Our temperature values obtained in this study are narrowly restricted between 1.5

and 3 MeV.

E. α-particles and nuclear clusterization

An observation concerns the large abundance of α-particles, already stressed in a previous paper for the same reaction at 60 A.MeV [7]. As it will be shown in a separate paper and already presented in a preliminary way [6], a great amount of them originates from the break-up of light nuclei as well from the decay of the excited primary PLF and TLF remnants. In any case, their abundance in this reaction is comparable or even higher than the abundance of protons.

The intrigant behavior of the temperature parameter T_{alpha} for the INT source (Fig. 10) appeals for some speculations. The T_{alpha} values decrease with the decrease of Z_{PLF} from 15 down to around 10 MeV for low Z_{PLF} while the T_i values for other LP stay constant around 15 MeV. For these low Z_{PLF}, the overlap is strong and if α-clusters are assumed existing in this piece of nuclear matter they could have more difficulties to escape than the other LP of smaller sizes. They could escape only after some cooling following the depletion of this region and hence T_{alpha} values would be lower. For peripheral collisions (large Z_{PLF}), less overlap is expected and these α-particles could escape as easily as the others and exhibit the same T values, as seen in Fig. 10. This effect does not manisfest itself on the multiplicities, probably because of the size variation of the overlap region.

Another interesting result [45] is the need to take into account two extra sources to reproduce the precise characteristics of the mid-rapidity emitted α-particles. Their velocities are close to the nucleon-α and α-nucleon ones. This kind of five-source analysis, not attempted in the present work, was made possible because of the use of 4π detector data.

These observations make legitimate to ask ourselves if they cannot be regarded as an experimental evidence of the preformation of clusters inside nuclei and how the predictions of models would change when taking this effect into account [48].

V. CONCLUSION

We have presented the light particle-fragment coincidences for the reaction $^{40}Ar +^{27} Al$ at 44 A.MeV. We have shown that our experimental method and a three-source analysis are very powerful in determining the fraction of particles that can hardly be associated with a source having either the projectile or the target velocity. For protons produced in peripheral interactions this fraction is of the order of 25%-35%, in agreement with the value predicted by recent Landau-Vlasov calculations [18]. In this context these protons could be identified with the prompt protons dynamically emitted in the first stages of the reaction. However, the fact that other complex particles, like α-particles, show up similar features, call into question the very simplistic way of treating the nucleus as formed only by nucleons, and must encourage theorists to take explicitely into account nuclear clusters in their calculations. Concerning the sources with projectile and target velocities, we were not able to fit the data with a unique set of parameters: the results, and in particular the extracted temperatures, depend on the particle nature. We suggest that the vicinity in phase space of the intermediate source respectively to the PLF and TLF sources could be the origin of this dependence, and consequentely we call for caution when using a thermodynamical formalism and the concept of "full equilibrium" in a range of energy where the "non equilibrated" processes are expected to become substantial.

To answer, now, the question that was the aim of this experiment, i.e. to have a comprehensive insight on the reaction scenario, our conclusion is the following. The collision gives origin primarily to a highly perturbated zone of nuclear matter, from which particles or clusters of intermediate velocity escape. In our simple approach we "simulate" this complex source with an "equilibrated" maxwellian energy distribution with volume emission, having half the velocity of the projectile and a temperature parameter of approximately 15-17 MeV. The parts of the projectile and of the target that are spatially less involved in the overlap zone, bring memory of the entrance reaction channel along their way-out from this interaction zone. These two remnants of the reaction, that we have called PLF and

TLF, are also sources of particles, that we have approximated with two equilibrated surface maxwellians, with velocity close respectively to the initial projectile and target velocities. The fact that their velocity and their temperature parameters are slightly depending on the PLF charge (impact parameter) and on the nature of the accompanying light particles, can be thought as an evidence that these remnants are not "fully" spectators, though this simplifying image is useful and approximately compatible with a great deal of data. Furthermore, the low LCP multiplicities accompanying these remnants, are in favor of PLF and TLF production with low excitation energies. In other words, our data corroborate the scenario of a participant-spectator mechanism, already invoked to explain the main PLF features of inclusive measurements at intermediate energies [26,50] in which, however, the interplay between "the participants" and "the spectators" cannot be completely neglected. As a consequence of this study and in agreement with [18], we conclude also that the presence of dynamical non-equilibrated processes in the overlap zone of the two interacting nuclei prevents the formation of very highly excited nuclei at these intermediate energies.

ACKNOWLEDGEMENTS

We wish to thank the Ganil machine staff for having provided us with a beam of excellent characteristics. We are also grateful to N. Giudice, N. Guardone, V. Sparti, S. Urso and J.L. Vignet for their assistance during the experiment, and to C. Marchetta for targets preparation.

REFERENCES

[1] T. C. Awes, S. Saini, G. Poggi, C. K. Gelbke, D. Cha, R. Legrain, G. D. Westfall, *Phys. Rev.* **C25** (1982) 2361.

[2] B. V. Jacak, G. D. Westfall, G. M. Crawley, D. Fox, C. K. Gelbke, L. H. Harwood, B. E. Hasselquist, W. G. Lynch, D. K. Scott, H. Stöcker, M. B. Tsang, G. Buchwald, *Phys. Rev.* **C35** (1987) 1751.

[3] D. Guerreau: "Light particle emission as probe of reaction mechanism and nuclear excitation", Int. School of Physics, Varenna (Italy) 1989 and Ganil-draft P89-17.

[4] J. Galin: "Hot nuclei studied with high efficiency neutron detectors", XXI Summer School on Nucl. Phys., Mikolajki(Poland), 1990 and Ganil-report P90-17.

[5] M. Geraci, Doctoral Thesis (unpublished), Università di Catania, 1997.

[6] G. Lanzanò, E. De Filippo, M. Geraci, A. Pagano, S. Aiello, A. Cunsolo, R. Fonte, A. Foti, M. L. Sperduto, C. Volant, J. L. Charvet, R. Dayras, R. Legrain, in *Proceedings of the XXXV International Winter Meeting on Nuclear Physics, Bormio, Italy*, edited by I. Iori (Università degli Studi di Milano, Milano, 1997), p. 536.

[7] G. Lanzanò, A. Pagano, G. Blancato, E. De Filippo, M. Geraci, R. Dayras, B. Berthier, F. Gadi-Dayras, R. Legrain, E. Pollacco, B. Heusch, *Phys. Rev.* **C58** (1998) 281.

[8] H. Fuchs, K. Möhring, *Rep. Prog. Phys.* **57** (1994) 231, and references therein.

[9] J. L. Wile et al , *Phys. Rev.* **C45** (1992) 2300.

[10] C. P. Montoya et al., *Phys. Rev. Lett.* **73** (1994) 3070.

[11] J. Péter et al., *Nucl. Phys.* **A593** (1995) 95.

[12] J. F. Dempsey et al , *Phys. Rev.* **C54** (1996) 1710.

[13] O. Dorvaux et al., *Nucl. Phys.* **A651** (1999) 225.

[14] Y. Larochelle et al., *Phys. Rev.* **C59** (1999) R565.

[15] E. Plagnol et al., INDRA collaboration, *Phys. Rev.* **C61** (2000) 014606.

[16] T. Lefort et al., INDRA collaboration, *Nucl. Phys.* **A662** (2000) 397.

[17] D. Doré et al., INDRA collaboration, in *Proceedings of the XXXVI International Winter Meeting on Nuclear Physics, Bormio, Italy*, edited by I. Iori (Università degli Studi di Milano, Milano, 1998), p. 381.
D. Doré et al., INDRA collaboration, submitted to *Phys. Lett. B.*

[18] Ph. Eudes, Z. Basrak, F. Sebille, *Phys. Rev.* **C56** (1997) 2003.

[19] G. Lanzanò, E. De Filippo, A. Pagano, "Detectors for Nuclear Physics Experimental activity at INFN Sezione di Catania", Proceedings of the Workshop, Acireale (Catania) March 24, 1993, pag. 10, edited by S. Aiello, A. Palmeri, F. Riggi., INFN Catania.

[20] G. Lanzanò, A. Pagano, E. De Filippo, E. Pollacco, R. Barth, B. Berthier, E. Berthoumieux, Y. Cassagnou, Sl. Cavallaro, J. L. Charvet, A. Cunsolo, R. Dayras, A. Foti, S. Harar, R. Legrain, V. Lips, C. Mazur, E. Norbeck, S. Urso, C. Volant, *Nucl. Instr. and Meth.* **A323** (1992) 694.

[21] E. De Filippo, R. Fonte, G. Lanzanò, A. Pagano, *Nuovo Cimento* **107A** (1994) 775.

[22] G. Lanzanò, A. Pagano, S. Urso, E. De Filippo, B. Berthier, J. L. Charvet, R. Dayras, R. Legrain, R. Lucas, C. Mazur, E. Pollacco, J. E. Sauvestre, C. Volant, C. Beck, B. Djerroud, B. Heusch, *Nucl. Instr. and Meth.* **A312** (1992) 515.

[23] T. Matulewicz, E. Grosse, H. Emling, H. Grein, R. Kulessa, F. M. Baumann, G. Domogala, H. Freiesleben, *Nucl. Instr. and Meth.* **A274** (1989) 501.

[24] G. Lanzanò, E. De Filippo, M. Geraci, A. Pagano, S. Urso, N. Colonna, G. D'Erasmo, E. M. Fiore, A. Pantaleo, Nuovo Cimento **110A** (1997) 505.

[25] J. P. Bondorf, *Journal de Physique* **C4** (1986) 263.

[26] R. Dayras, A. Pagano, J. Barrette, B. Berthier, D. M. de Castro Rizzo, E. Chavez, O. Cisse, R. Legrain, M.C. Mermaz, E. C. Pollacco, H. Delagrange, W. Mittig, B. Heusch, R. Coniglione, G. Lanzanò, A. Palmeri, *Nucl. Phys.* **A460**, (1986) 299.

[27] A. S. Goldhaber, *Phys. Rev.* **C17** (1978) 2243.

[28] V. F. Weisskopf, *Phys. Rev.* **52** (1937) 295.

[29] R. Dayras, R. Coniglione, J. Barrette, B. Berthier, D. M. de Castro Rizzo, O. Cisse, F. Gadi, R. Legrain, M. C. Mermaz, H. Delagrange, W. Mittig, B. Heusch, G. Lanzanò, A. Pagano, *Phys. Rev. Lett.* **62** (1989) 1017.

[30] A. Albergo, S. Costa, E. Costanzo, A. Rubbino, *Nuovo Cimento* **A 89** (1985) 1.

[31] R. A. Kryger, A. Azhari, E. Ramakrishnan, M. Thoennessen, S. Yokoyama, *Nucl. Instr. and Meth* **A346** (1994) 544.

[32] O. Dorvaux et al., *Proceedings of the 8^{th} International Conference on Nuclear Reaction Mechanisms*, Varenna 1997, Ricerca Scientifica ed Educazione Permanente, ed. by E. Gadioli, Suppl. 111 p. 336.

[33] J. Pochodzalla et al., *Phys. Rev. Lett.* **75** (1995) 1040.

[34] M. B. Tsang et al., *Phys. Rev.* **C53** (1996) R1057.

[35] X. Campi, H. Krivine, E. Plagnol, *Phys. Lett.* **B385** (1996) 1.

[36] Y.-G. Ma et al., INDRA collaboration, *Phys. Lett.* **B390** (1997) 41.

[37] K. Kwiatkowski, A. S. Botvina, D. S. Bracken, E. Renshaw Foxford, W. A. Friedman, R. G. Korteling, K. B. Morley, E. C. Pollacco, V. E. Viola, C. Volant, *Phys. Lett.* **B423** (1998) 21.

[38] W. Trautmann, ALADIN collaboration, in *Advances in Nuclear Dynamics 4*, edited by Bauer et Ritter, Plenum Press, New York, 1998 p. 349 and references therein.

[39] R. Dayras, Program ABRADE, unpublished.

[40] G. Lanzanò, A. Pagano, E. De Filippo, R. Dayras, R. Legrain, *Z. Phys.* **A343** (1992) 429.

[41] J. P. Bondorf, J. De, G. Fai, A. O. T. Karvinen, *Nucl. Phys.* **A430** (1984) 445.

[42] A. Bonasera, M. Di Toro, C. Grégoire, *Nucl. Phys.* **A463** (1987) 653.

[43] J. J. Gaimard, K. H. Schmidt, *Nucl. Phys.* **A531** (1991) 709.

[44] J. Pochodzalla et al., Proceedings of CRIS '96, Acicastello, Italy, 1996, pag. 1-22. Edited by S. Costa, S. Albergo, A. Insolia, C. Tuvè, Università di Catania and INFN, Italy, World Scientific.

[45] A. Hürstel et al., INDRA collaboration, *Proceedings of the XXXVIII International Winter Meeting on Nuclear Physics, Bormio, Italy*, edited by I. Iori (Università degli Studi di Milano, Milano, 2000), to appear.

[46] P. Pawłowski et al., INDRA collaboration, submitted to *Phys. Rev. C* .
D. Doré et al., INDRA collaboration, in preparation.

[47] M. F. Rivet et al., INDRA collaboration, *Phys. Lett.* **B388** (1996) 219.
B. Borderie et al., INDRA collaboration, *Phys. Lett.* **B388** (1996) 224.

[48] P. E. Hodgson, Acta Phys. Hung. New Ser.: Heavy Ion Phys. 2 (1995) 199 and references therein.

[49] J. Barrette et al., Note CEA-N2437 (1985) p. 96-101.

[50] G. Lanzanò, E. De Filippo, A. Pagano, E. Berthoumieux, R. Dayras, R. Legrain, E. C. Pollacco, C. Volant, *Phys. Lett.* **B332** (1994) 31.

TABLE CAPTION

Tab. 1 The source parameters (velocity v_s, temperature T, Coulomb parameter v_c and intensity σ) are given in table I respectively for PLF, TLF and intermediate sources, relatively to a) protons, deuterons, tritons, b) ^3He and α-particle in coincidence with projectile-like fragments of charge from Z=7 up to Z=19. Absolute values for the source intensity are obtained by using previous light charged particle [49] and PLF [26] inclusive angular distribution data for the same reaction and taking into account the finite efficiency of the forward wall for PLF detection, as described in [5]. Numbers between parentheses are the Z_{PLF} absolute cross-sections (in mb) taken from [26].

Tab. 2 The so-called "isotopic-temperature" (in MeV), not corrected for secondary decay from unbound excited states of heavier fragments [34,35], is reported for each one of the three sources as a function of the coincident PLF charge, by using three different combinations of light particle intensities from table I, respectively:

$$T_1 = \frac{14.3}{ln\left[\frac{\sigma(d)\sigma(^4He)}{\sigma(t)\sigma(^3He)}\times 1.6\right]}, T_2 = \frac{4.033}{ln\left[\frac{\sigma(d)\sigma(d)}{\sigma(p)\sigma(t)}\times 3.464\right]}, T_3 = \frac{18.35}{ln\left[\frac{\sigma(p)\sigma(^4He)}{\sigma(d)\sigma(^3He)}\times 5.55\right]}$$

FIGURE CAPTION

Fig. 1 Experimental set-up, constituted by a 60-phoswich forward wall (distance to the target 233 cm, angular range from 0.75° to 7°), a 18-phoswich backward wall (distance to the target 50 cm, angular range from 160° to 175°) and a battery of 30-in plane phoswichs on both sides with respect to the beam direction (variable distance to the target from 200 cm in the forward direction to 50 cm in the backward direction, angular range from 10° to 150°). See text for details.

Fig. 2 Lorentz invariant cross-section bidimensional plot for α-particles in coincidence with forward wall fragments of charge Z=16.

Fig. 3 Lorentz invariant cross-section bidimensional plot for protons in coincidence with forward wall fragments of charge from Z=4 to Z=19.

Fig. 4 Moving source calculations for neutrons (upper part) and protons (middle part) for surface (full curve) and volume emission (dashed curve) at θ=0° and θ=20° in the laboratory system. The source and Coulomb velocities are v_s=8 cm/ns and v_c=1 cm/ns respectively. Lower part: velocity distribution for protons in the emitter frame calculated by formula 1a) and 1b).

Fig. 5 Experimental (non-normalized) α-particle velocity spectra from θ=1.5° to θ=172°, in coincidence with projectile-like fragments of charge Z=14 detected in the forward wall. The lines are the result of a three equilibrated sources fit procedure (see text). Target-like fragment source: dotted line; projectile-like fragment source: dashed line; intermediate source: dot-dashed line; total: thick line. The beam velocity is 8.9 cm/ns.

Fig. 6 As Fig. 5, but only for some selected laboratory angles and for all types of particles. Note for neutrons the lack of experimental data at θ=4.2°.

Fig. 7 As Fig. 5, but at a fixed angle (θ=4.2°) and for coincidences between protons and projectile-like fragments of charge from Z=9 up to Z=19.

Fig. 8 The velocity of PLF and TLF sources, as deduced from the fit procedure, are reported as a function of the PLF charge for different emitted LP.

Fig. 9 The PLF Coulomb parameter B_c, as deduced from the fit procedure, is reported as a function of the PLF charge for different emitted LCP.

Fig. 10 The temperature parameter T for different particles (p, d, t, ^{4}He, n) and for the three sources (full circles, PLF source; open circles, TLF source; stars, intermediate source) is reported as a function of the PLF charge. The predictions of isotopic ratios formula involving dα-t^{3}He particles are reported for PLF (full line), TLF (dashed line) and intermediate (dotted line) sources respectively.

Fig. 11 Light charged particles multiplicities as a function of the Z_{PLF} for the three different sources.

Fig. 12 The reconstructed (see text) primary PLF charge Z^*_{PLF} and excitation energy are shown, respectively, in a) and b) (data, full points) as a function of the detected PLF charge Z_{PLF}. In a) the dashed line indicates the beam atomic number, while the squares are the predictions taken from Fig. 11 of [18], concerning the production of primary and secondary PLF, for the same reaction ^{40}Ar+^{27}Al at 65 A.MeV. Also shown are the mean primary PLF charges predicted by a simple abrasion-ablation model as described in [26,39,40] (open circles). In b) the predictions of the geometrical abrasion model and the results of [29] for a binary reaction mechanism are shown respectively by open circles and full stars for the same system. Lines are drawn only to guide the eye. In c) the temperature parameter T, as extracted by the fit procedure described in the text, is reported only for protons (full circles) and α-particles (circles), as a function of the excitation energy per nucleon (see text). The same dependence is shown for the temperature deduced from a standard Fermi-gas model with level density parameter a=12 (dotted line) and a=8 (dashed line). Errors bars of 20 percent are drawn for the excitation energies in b) and c). They represent estimates of the accuracy of the

calorimetry method used.

Fig. 13 The relative intensity of PLF (full lines), TLF (dashed lines) and intermediate source INT (dotted lines) is reported as a function of the PLF charge for protons, deuterons, tritons and α-particles. In the case of protons we report also the predictions of [18] concerning the intermediate source INT (dots), for the same reaction ^{40}Ar+^{27}Al at 65 A.MeV.

TABLES

TABLE I.

(a)	PLF source				TLF source			INT source	
	v_s (cm/ns)	T (MeV)	σ (mb)	v_c (cm/ns)	v_s (cm/ns)	T (MeV)	σ (mb)	T (MeV)	σ (mb)
p-Z σ_{PLF}									
7 (90)	7.8	4.2	103.2	0.0	0.9	4.8	49.3	14.1	110.4
8 (90)	7.7	4.1	111.8	0.0	1.0	4.8	49.8	14.4	96.7
9 (65)	7.8	4.3	78.0	0.2	1.0	4.9	38.2	14.4	57.9
10 (90)	7.8	4.2	116.4	0.3	1.0	4.7	55.6	14.2	87.4
11 (95)	7.9	4.1	118.1	0.4	1.0	4.5	62.1	14.9	73.3
12 (130)	8.0	3.7	156.5	0.6	0.9	4.3	75.6	14.5	102.1
13 (130)	8.0	3.6	141.0	0.9	0.8	4.0	82.7	14.6	80.9
14 (190)	8.1	3.4	164.3	0.9	0.7	3.6	104.5	13.6	96.9
15 (180)	8.2	3.2	121.0	1.2	0.6	3.3	100.2	14.6	64.4
16 (290)	8.3	2.8	114.3	1.2	0.5	2.9	107.3	13.8	74.2
17 (300)	8.4	2.8	75.2	1.3	0.4	2.7	94.9	14.7	49.2
18 (160)	8.4	2.4	30.0	1.4	0.2	2.4	43.9	14.7	27.3
19 (10)	8.4	2.4	2.9	1.6	0.0	2.4	5.4	14.6	4.4
d-Z									
7	7.7	5.5	46.0	0.0	1.2	6.0	29.9	15.4	54.1
8	7.7	5.6	45.2	0.2	1.3	6.1	31.9	14.9	49.9
9	7.7	5.7	29.5	0.2	1.2	6.3	19.7	14.9	33.9
10	7.8	5.4	40.9	0.3	1.2	6.1	27.8	14.3	47.1
11	7.8	5.1	38.6	0.6	1.2	6.1	25.0	14.1	45.8
12	7.9	4.9	44.4	0.7	1.1	5.7	31.4	14.4	61.2
13	7.9	4.7	36.3	0.8	1.0	5.5	28.1	14.8	50.6

14	8.0	4.6	37.3	0.9	0.9	5.3	31.2	13.9	53.8
15	8.1	4.1	21.8	1.1	0.8	4.8	20.9	14.3	38.7
16	8.1	4.0	17.2	1.1	0.7	4.5	21.8	14.3	32.7
17	8.2	3.8	7.8	1.3	0.5	4.1	14.4	15.4	23.9
18	8.4	3.5	1.7	1.3	0.4	3.9	6.0	16.0	10.4
19	8.5	3.4	0.1	1.4	0.1	3.7	0.9	16.0	2.1
t-Z									
7	7.6	6.1	23.8	0.0	1.4	7.0	13.8	17.5	22.5
8	7.5	6.2	23.1	0.0	1.4	6.9	14.8	16.2	24.8
9	7.6	6.5	14.3	0.2	1.5	7.2	10.6	15.6	14.7
10	7.6	6.3	19.6	0.3	1.5	7.2	13.6	14.4	21.3
11	7.7	6.1	16.8	0.3	1.5	6.8	15.1	14.8	20.5
12	7.8	5.9	19.5	0.5	1.4	6.6	20.2	15.2	28.3
13	7.9	5.5	14.2	0.6	1.3	6.4	13.9	14.6	24.9
14	7.9	5.3	14.1	0.6	1.2	6.1	15.9	14.6	28.1
15	8.1	4.8	7.4	0.7	1.1	5.7	8.6	15.2	20.3
16	8.2	4.4	4.7	0.9	0.9	5.3	7.2	15.7	17.4
17	8.3	4.0	1.9	0.9	0.6	4.6	4.3	16.0	10.1
18	8.4	3.8	0.4	1.0	0.4	4.4	1.6	16.0	3.5
19	8.6	3.4	0.1	1.0	0.2	4.1	0.3	16.0	1.5

(b)	PLF source				TLF source			INT source	
	v_s	T	σ	v_c	v_s	T	σ	T	σ
	(cm/ns)	(MeV)	(mb)	(cm/ns)	(cm/ns)	(MeV)	(mb)	(MeV)	(mb)
^{3}He-Z									
7	7.6	6.1	14.1	0.0	1.4	7.0	9.2	17.5	12.2
8	7.5	6.2	12.9	0.0	1.4	6.9	9.7	16.2	12.6
9	7.6	6.5	9.1	0.2	1.5	7.2	7.1	15.6	7.0
10	7.6	6.3	11.8	0.5	1.5	7.2	9.8	14.4	7.8
11	7.7	6.1	10.9	0.5	1.5	6.8	8.9	14.8	10.2
12	7.8	5.9	12.0	0.7	1.4	6.6	13.0	15.2	12.4
13	7.9	5.5	9.0	0.8	1.3	6.4	9.2	14.6	11.3
14	7.9	5.3	8.3	0.9	1.2	6.1	10.9	14.6	11.5
15	8.1	4.8	4.1	1.1	1.1	5.7	6.5	15.2	8.2
16	8.2	4.4	2.5	1.2	0.9	5.3	5.0	15.7	7.8
17	8.3	4.0	0.6	1.3	0.6	4.6	3.0	16.0	3.7
18	8.4	3.8	0.1	1.4	0.4	4.4	1.3	16.0	2.1
19	8.6	3.4	0.2	1.5	0.2	4.1	0.2	16.0	1.3
α-Z									
7	8.0	4.7	151.7	0.0	1.1	4.9	63.4	11.2	176.0
8	8.0	5.0	152.4	0.0	1.2	5.1	76.2	10.9	159.9
9	7.9	5.4	92.4	0.1	1.2	5.2	62.6	10.5	99.9
10	7.9	5.3	125.0	0.4	1.2	5.0	98.2	10.7	132.7
11	7.9	5.2	115.2	0.6	1.2	4.9	104.9	11.0	123.6
12	8.0	5.0	140.4	0.6	1.1	4.7	143.3	11.2	149.8
13	8.1	4.6	119.2	0.7	1.0	4.3	131.7	11.7	120.2
14	8.2	4.2	127.5	0.8	0.9	4.1	147.9	12.1	125.5

15	8.3	3.7	80.0	0.9	0.8	3.7	111.3	13.1	81.0
16	8.4	3.5	61.5	0.9	0.6	3.3	128.7	13.1	63.2
17	8.5	3.4	17.9	1.1	0.5	3.0	99.7	13.6	28.2
18	8.6	3.0	1.6	1.2	0.4	2.8	48.9	14.2	5.8
19	8.5	2.7	0.1	1.3	0.1	2.4	7.1	14.7	1.3

TABLE II.

	PLF source			TLF source			INT source		
Z	T_1	T_2	T_3	T_1	T_2	T_3	T_1	T_2	T_3
9	4.1	4.0	3.7	4.4	3.4	4.0	3.6	2.6	3.7
10	4.0	4.3	3.6	4.1	3.2	3.9	3.5	2.8	3.6
11	3.9	4.2	3.5	4.2	4.8	3.6	3.8	2.6	3.9
12	3.8	5.0	3.4	4.3	5.0	3.7	3.8	2.7	3.9
13	3.6	4.9	3.2	3.7	4.6	3.4	4.0	2.7	4.0
14	3.4	5.5	3.1	3.8	5.7	3.3	4.1	3.1	3.9
15	3.2	6.5	2.9	3.4	7.2	3.0	4.2	2.9	4.1
16	2.9	6.3	2.7	3.0	5.3	2.8	4.5	3.8	4.0
17	2.7	10.3	2.5	2.8	7.3	2.6	4.2	2.9	4.1

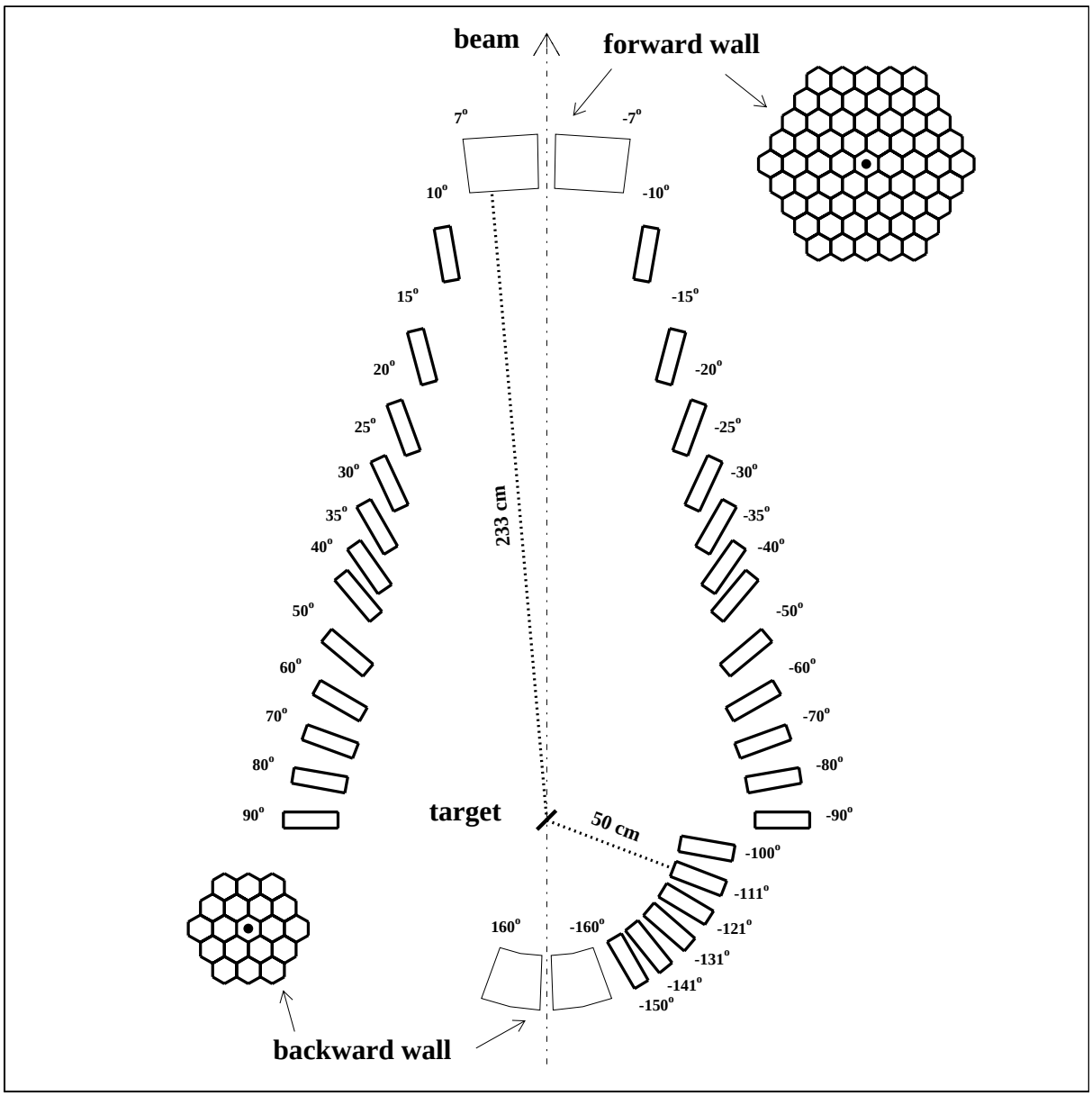
beam
forward wall
7°
-7°
10°
-10°
15°
-15°
20°
-20°
25°
-25°
30°
-30°
35°
-35°
40°
-40°
50°
-50°
60°
-60°
70°
-70°
80°
-80°
90°
-90°
233 cm
target
50 cm
-100°
-111°
-121°
-131°
-141°
-150°
160°
-160°
backward wall

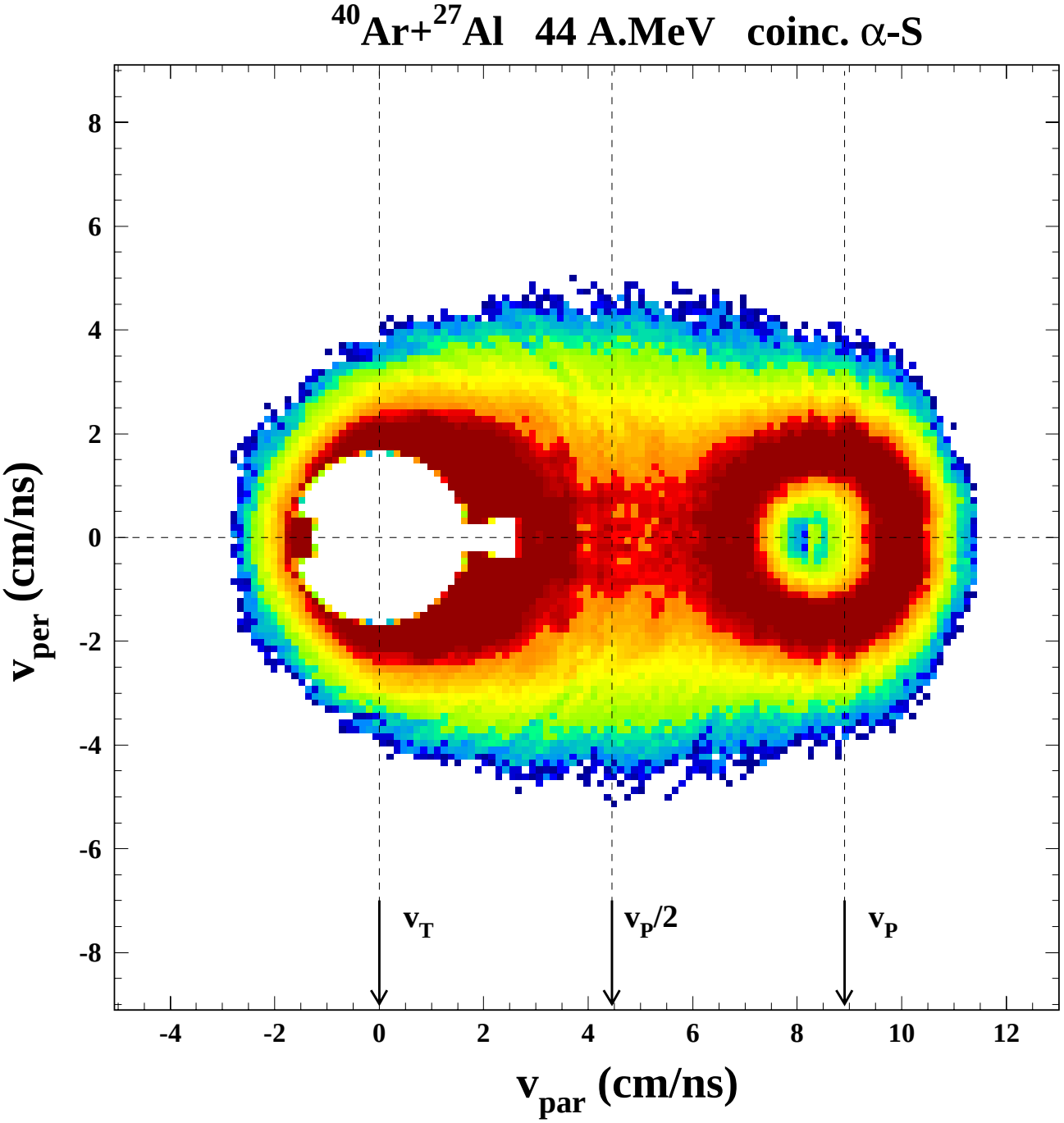
^{40}Ar+^{27}Al 44 A.MeV coinc. α-S
v_per (cm/ns)
v_par (cm/ns)
v_T
v_P/2
v_P
8
6
4
2
0
-2
-4
-6
-8
-4
-2
0
2
4
6
8
10
12

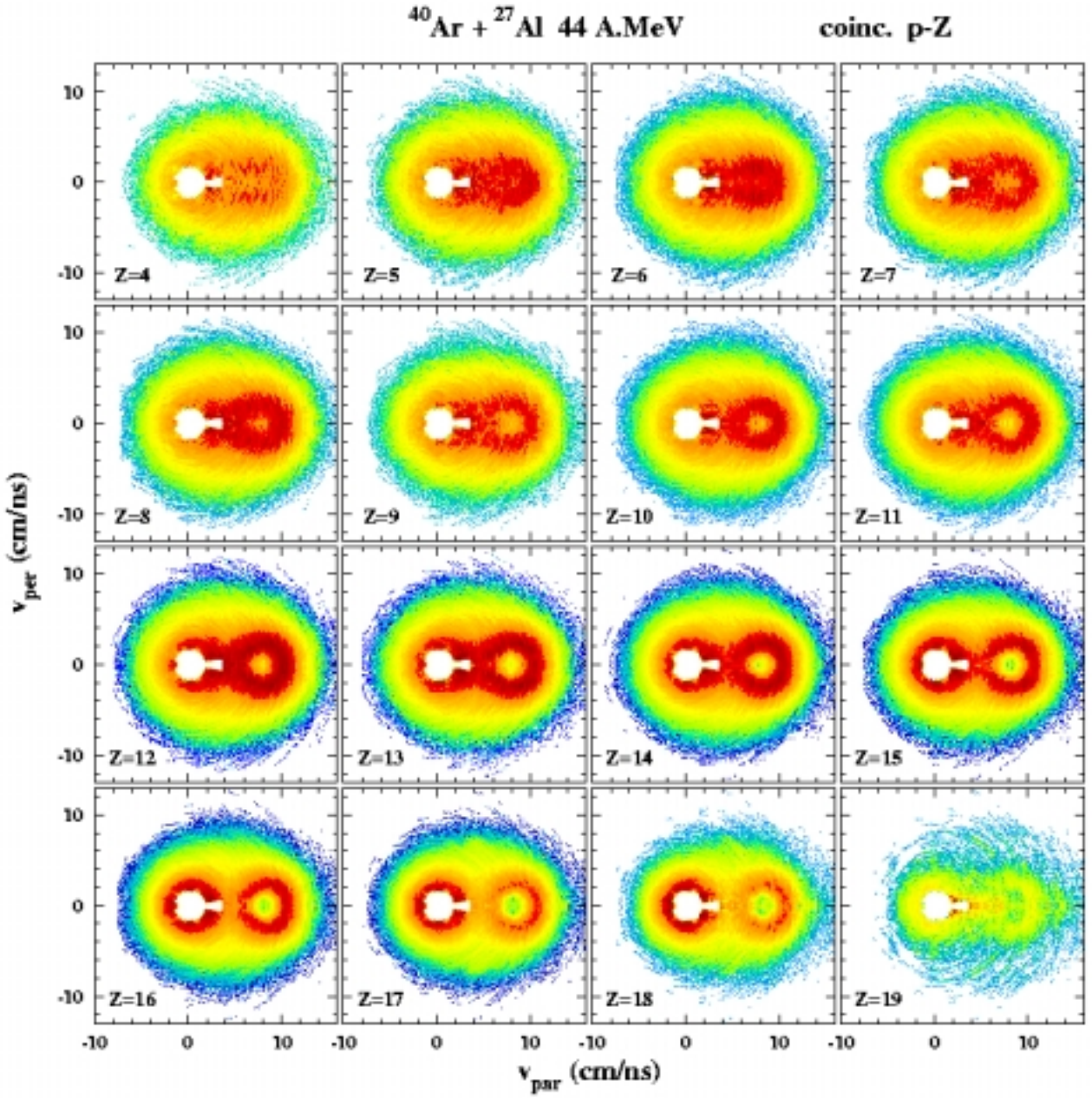
^{40}Ar + ^{27}Al 44 A.MeV
coinc. p-Z
Z=4
Z=5
Z=6
Z=7
Z=8
Z=9
Z=10
Z=11
Z=12
Z=13
Z=14
Z=15
Z=16
Z=17
Z=18
Z=19
v_{per} (cm/ns)
v_{par} (cm/ns)
10
0
-10

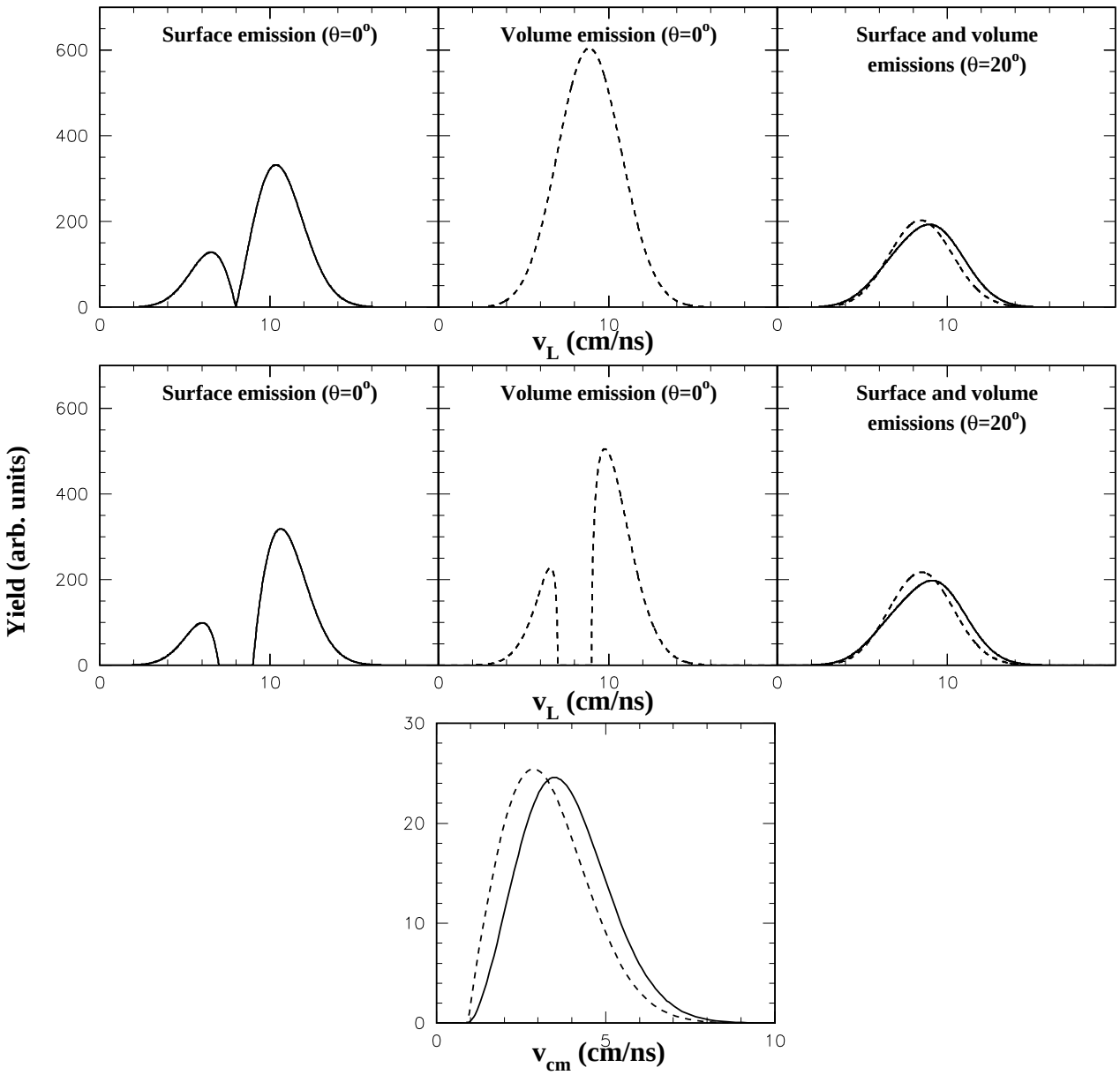
Surface emission (θ=0°)
Volume emission (θ=0°)
Surface and volume emissions (θ=20°)
Yield (arb. units)
v_L (cm/ns)
v_cm (cm/ns)

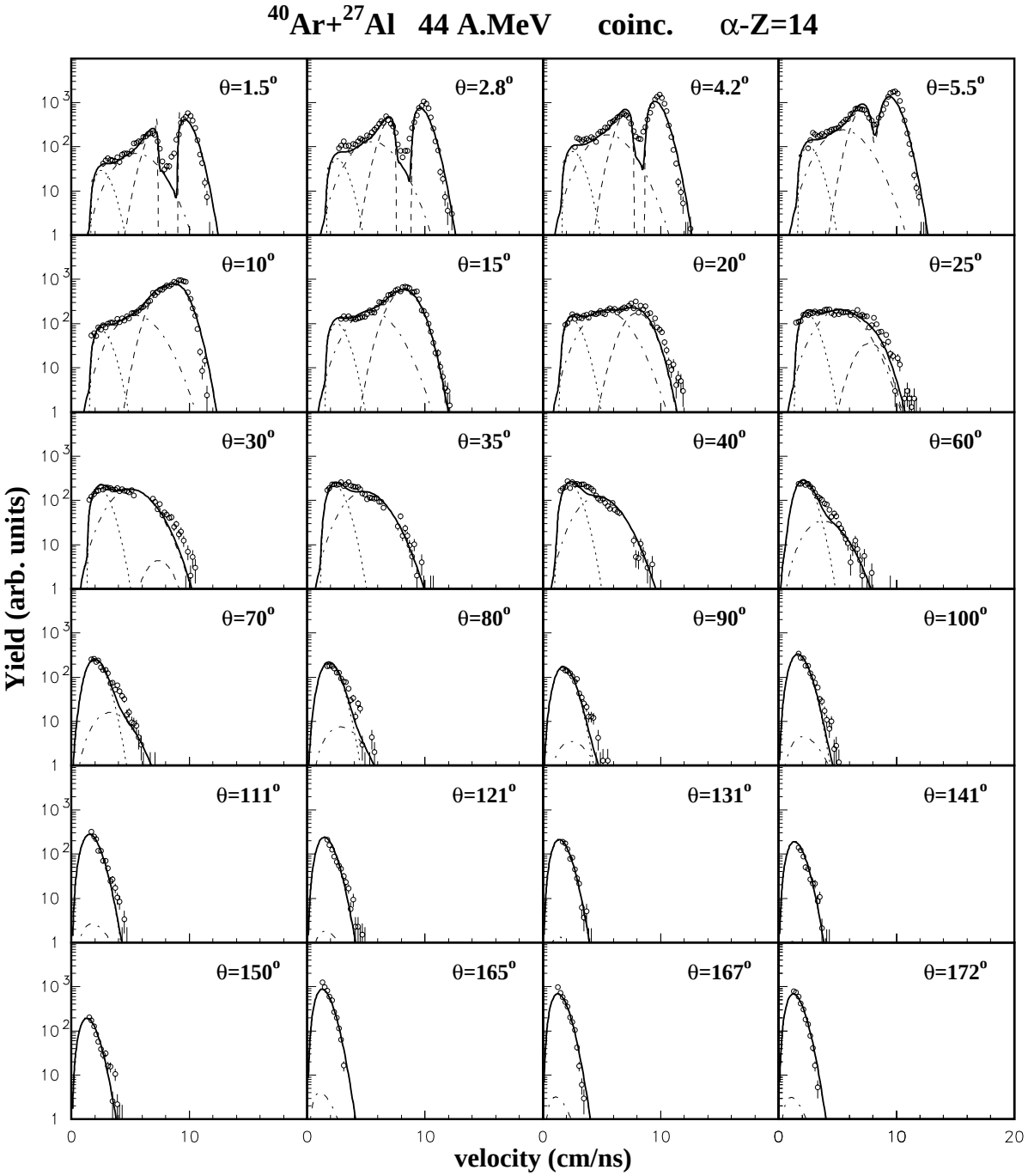
^{40}Ar+^{27}Al 44 A.MeV coinc. α-Z=14
θ=1.5°
θ=2.8°
θ=4.2°
θ=5.5°
θ=10°
θ=15°
θ=20°
θ=25°
θ=30°
θ=35°
θ=40°
θ=60°
θ=70°
θ=80°
θ=90°
θ=100°
θ=111°
θ=121°
θ=131°
θ=141°
θ=150°
θ=165°
θ=167°
θ=172°
Yield (arb. units)
velocity (cm/ns)

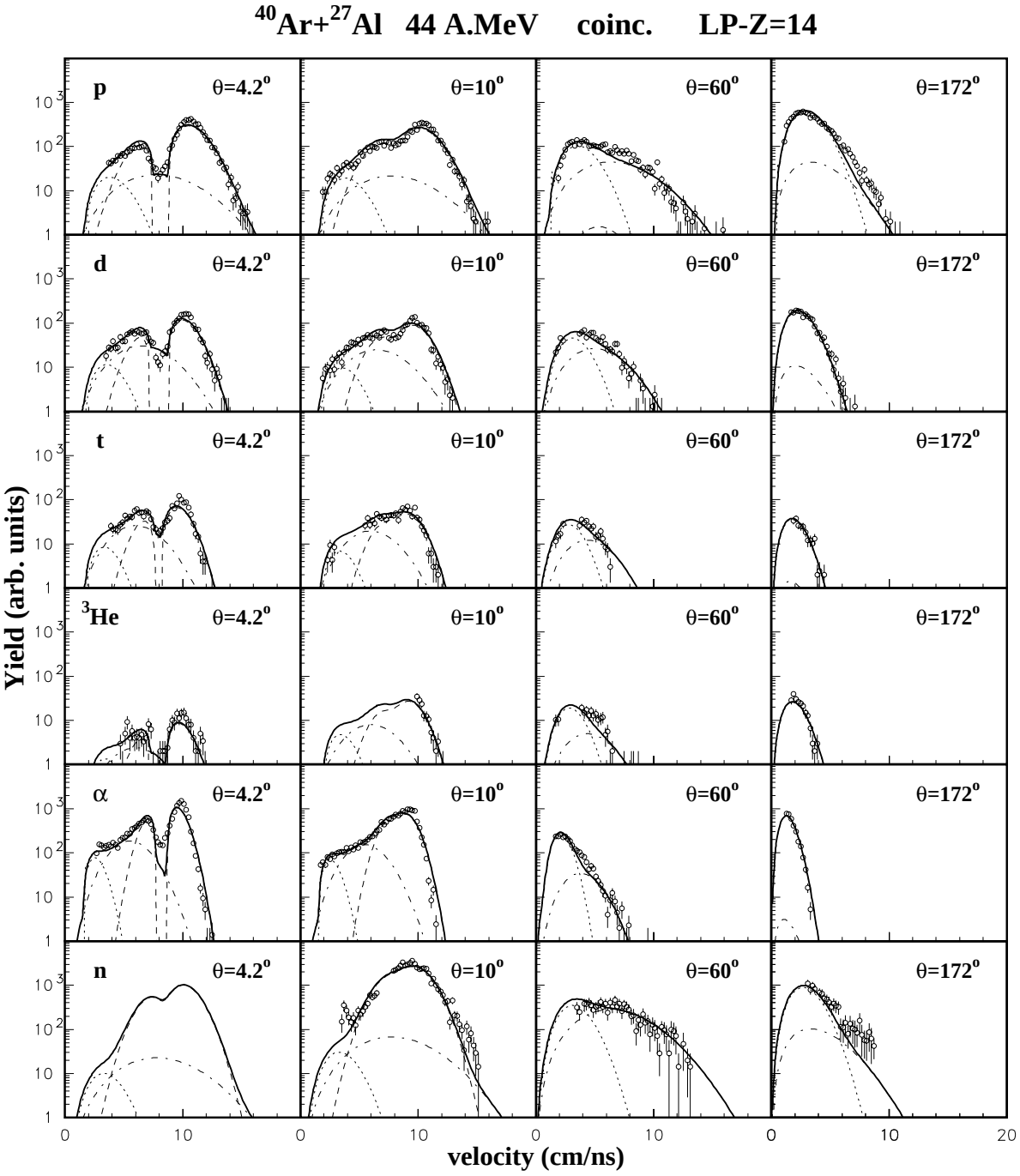
^{40}Ar+^{27}Al 44 A.MeV coinc. LP-Z=14
p
d
t
^{3}He
α
n
θ=4.2°
θ=10°
θ=60°
θ=172°
Yield (arb. units)
velocity (cm/ns)

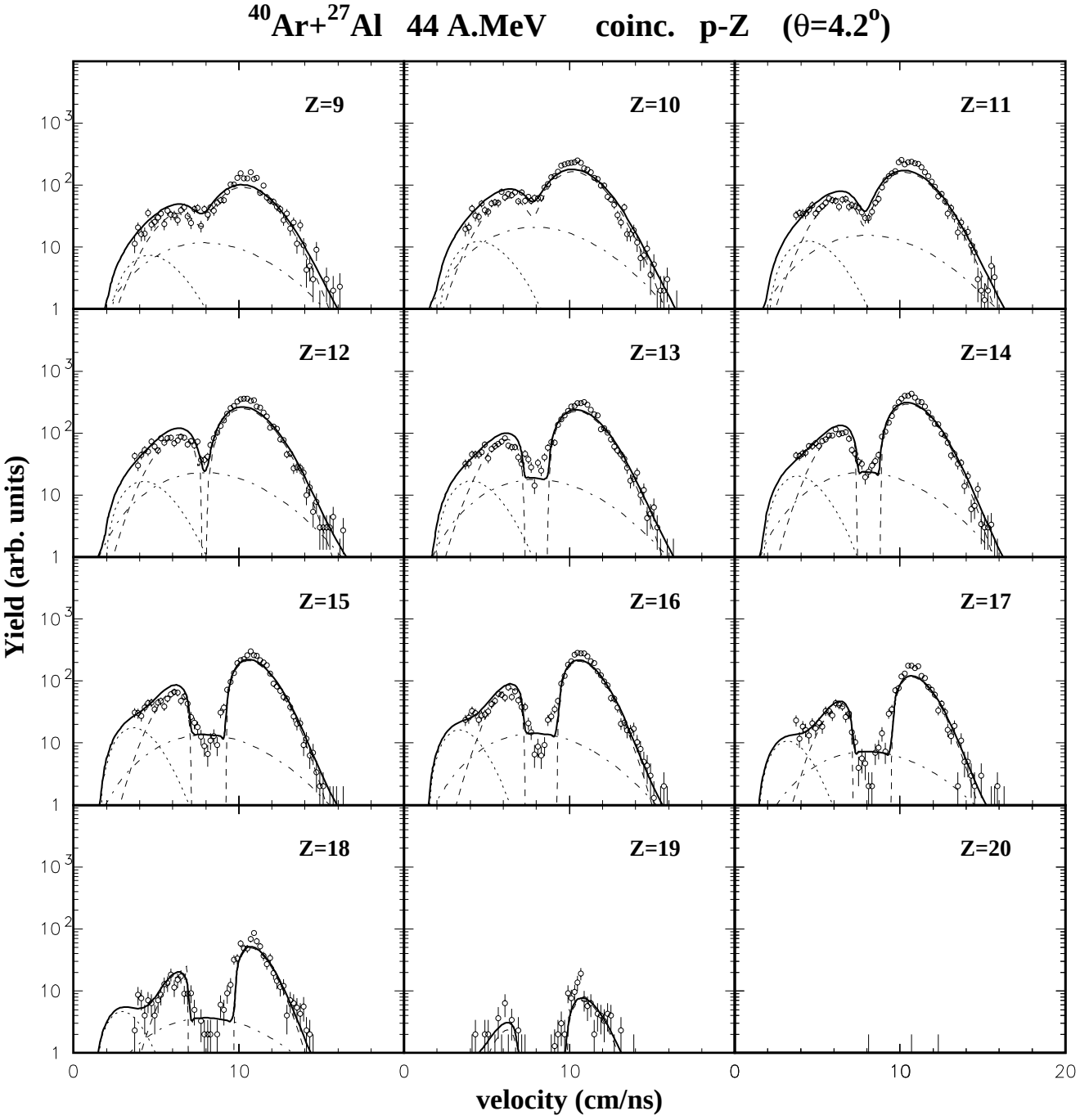
^{40}Ar+^{27}Al 44 A.MeV coinc. p-Z (θ=4.2°)
Z=9
Z=10
Z=11
Z=12
Z=13
Z=14
Z=15
Z=16
Z=17
Z=18
Z=19
Z=20
Yield (arb. units)
velocity (cm/ns)

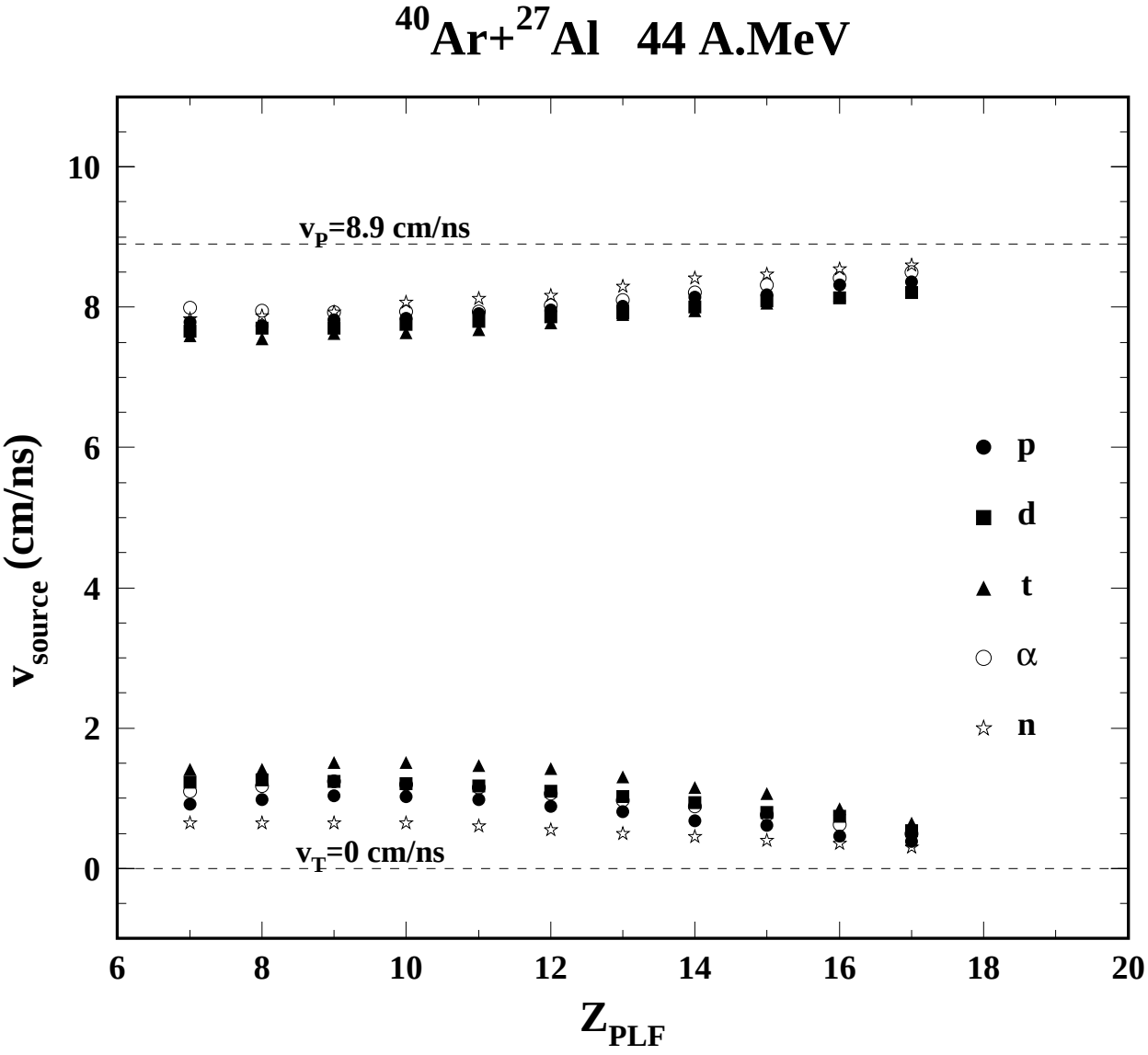
40Ar+27Al 44 A.MeV
vP=8.9 cm/ns
vT=0 cm/ns
p
d
t
α
n
vsource (cm/ns)
ZPLF
0
2
4
6
8
10
6
8
10
12
14
16
18
20

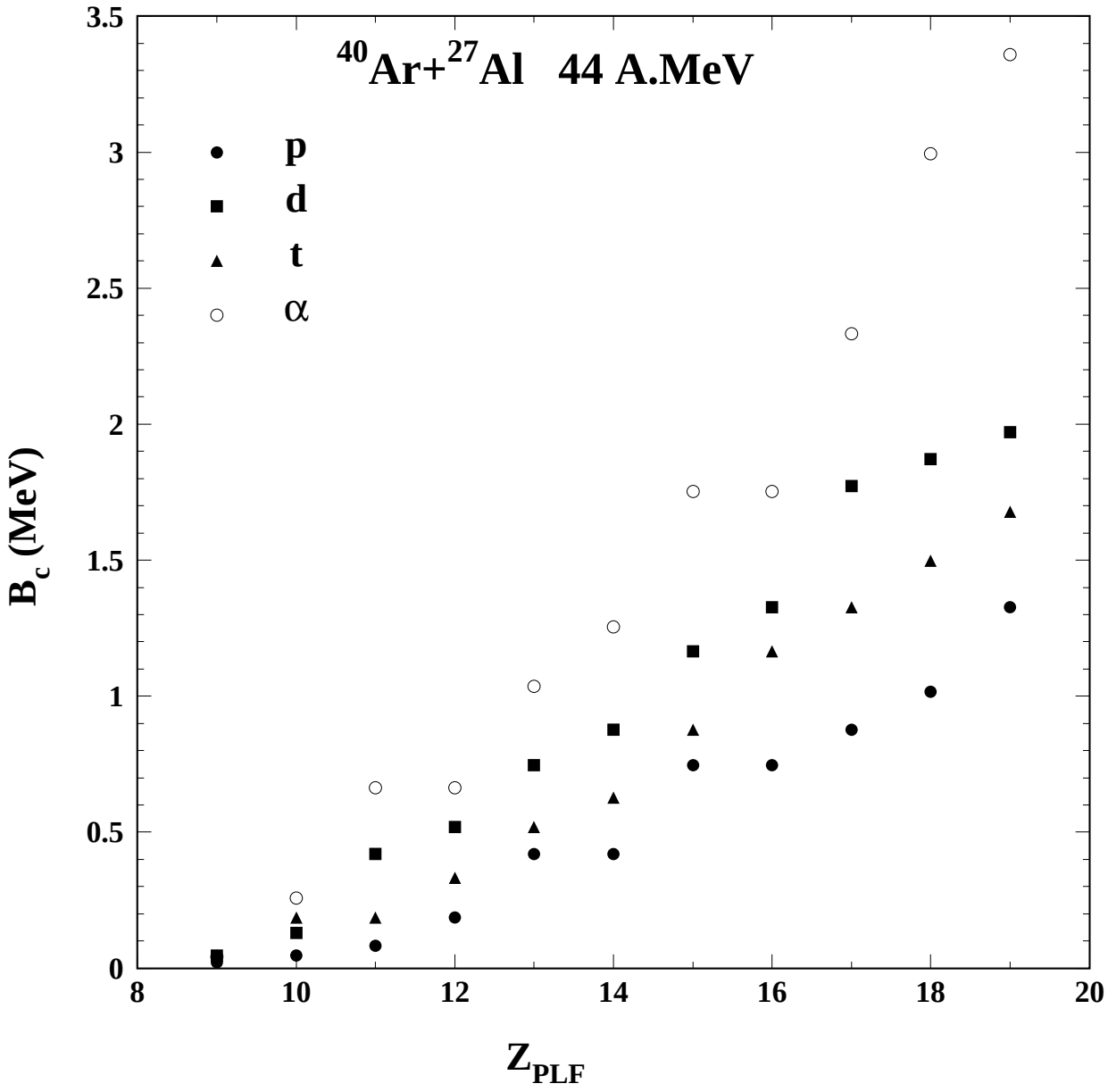
^{40}Ar+^{27}Al 44 A.MeV
p
d
t
α
B$_c$ (MeV)
Z$_{PLF}$
0
0.5
1
1.5
2
2.5
3
3.5
8
10
12
14
16
18
20

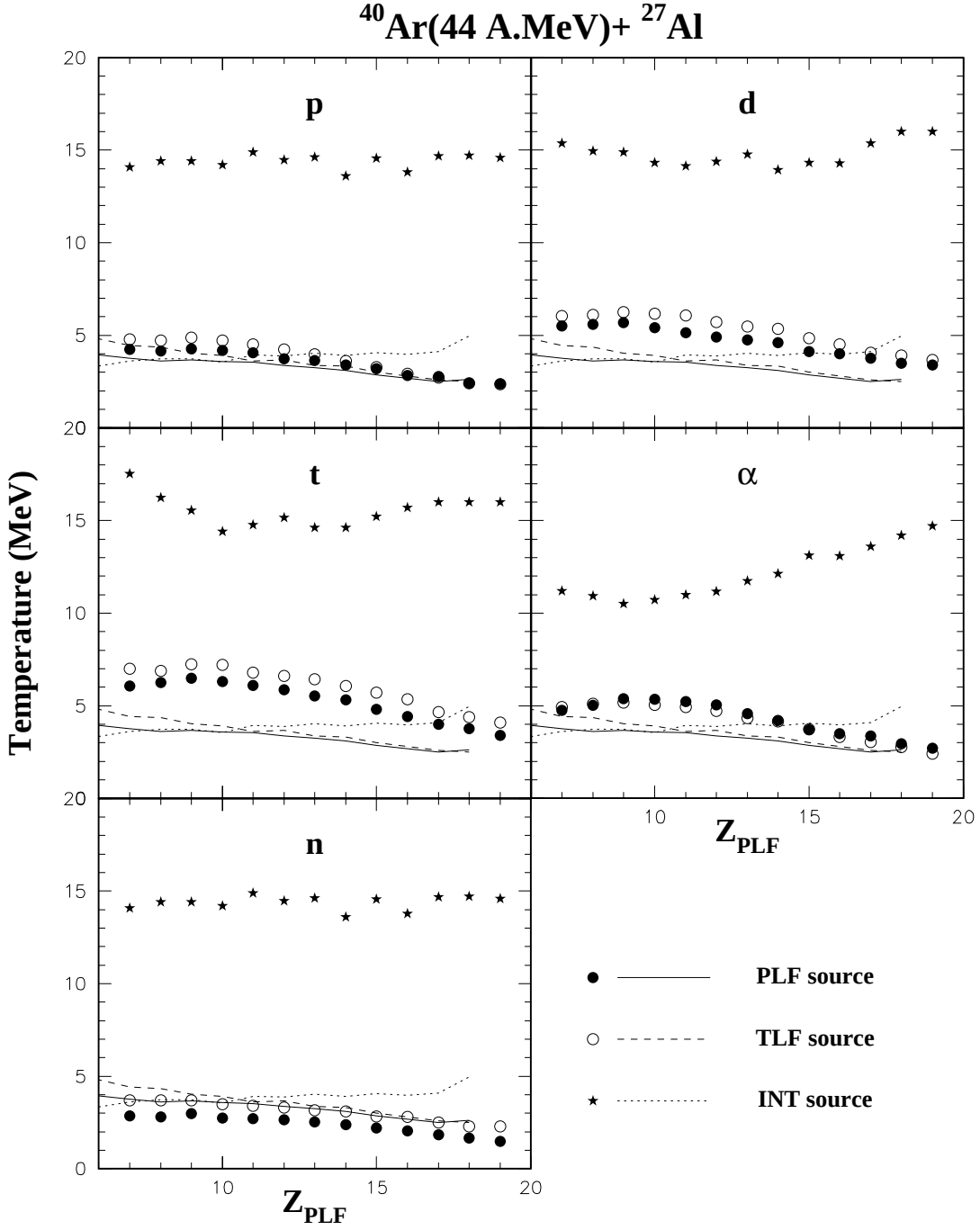
40Ar(44 A.MeV)+ 27Al
p
d
t
α
n
Temperature (MeV)
ZPLF
ZPLF
PLF source
TLF source
INT source

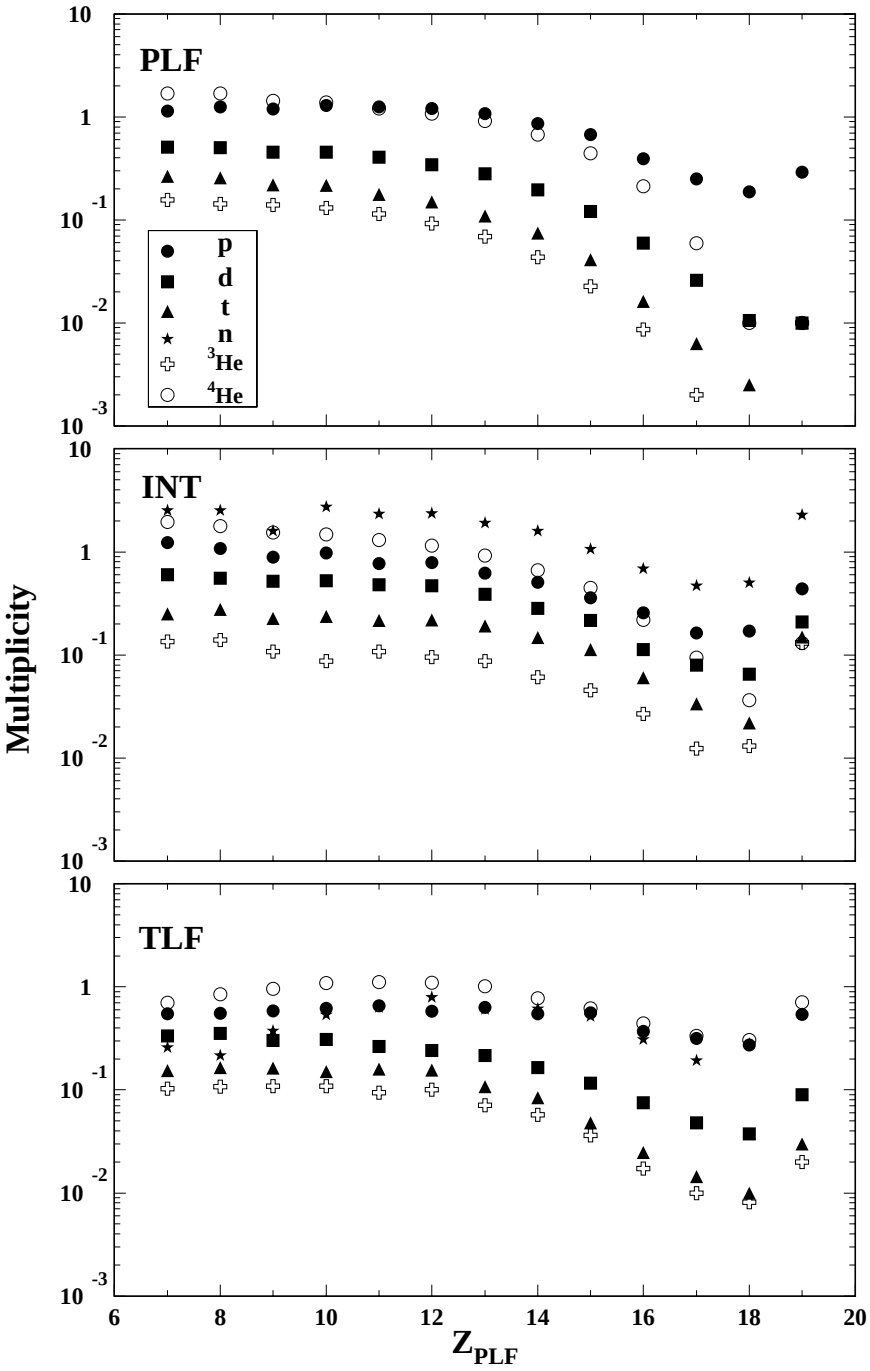
PLF
INT
TLF
p
d
t
n
3He
4He
Multiplicity
Z_PLF
10
1
10^-1
10^-2
10^-3
6
8
10
12
14
16
18
20

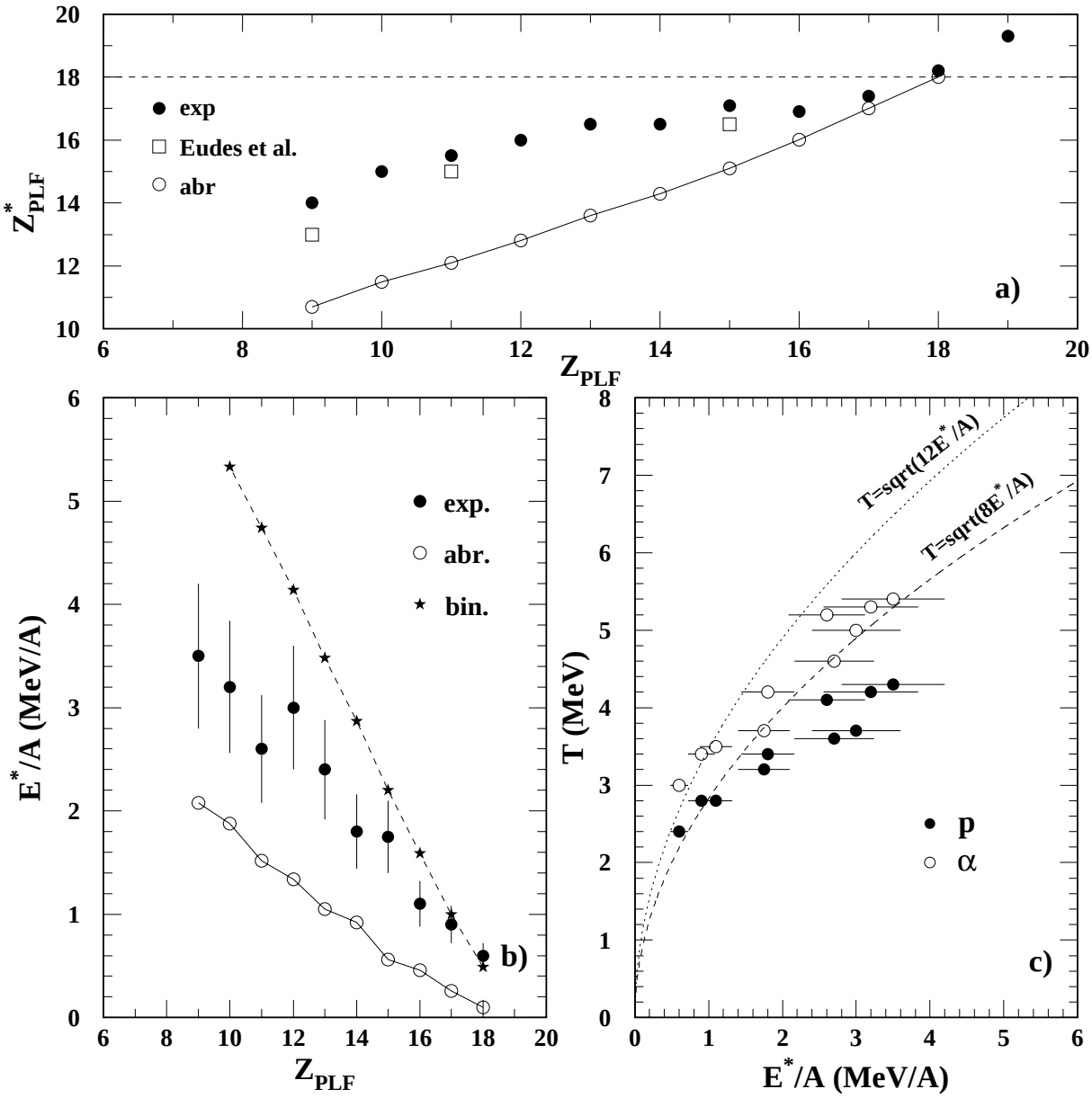
exp
Eudes et al.
abr
a)
Z^*_{PLF}
Z_{PLF}
exp.
abr.
bin.
b)
E^*/A (MeV/A)
Z_{PLF}
$T=sqrt(12E^*/A)$
$T=sqrt(8E^*/A)$
p
α
c)
T (MeV)
E^*/A (MeV/A)

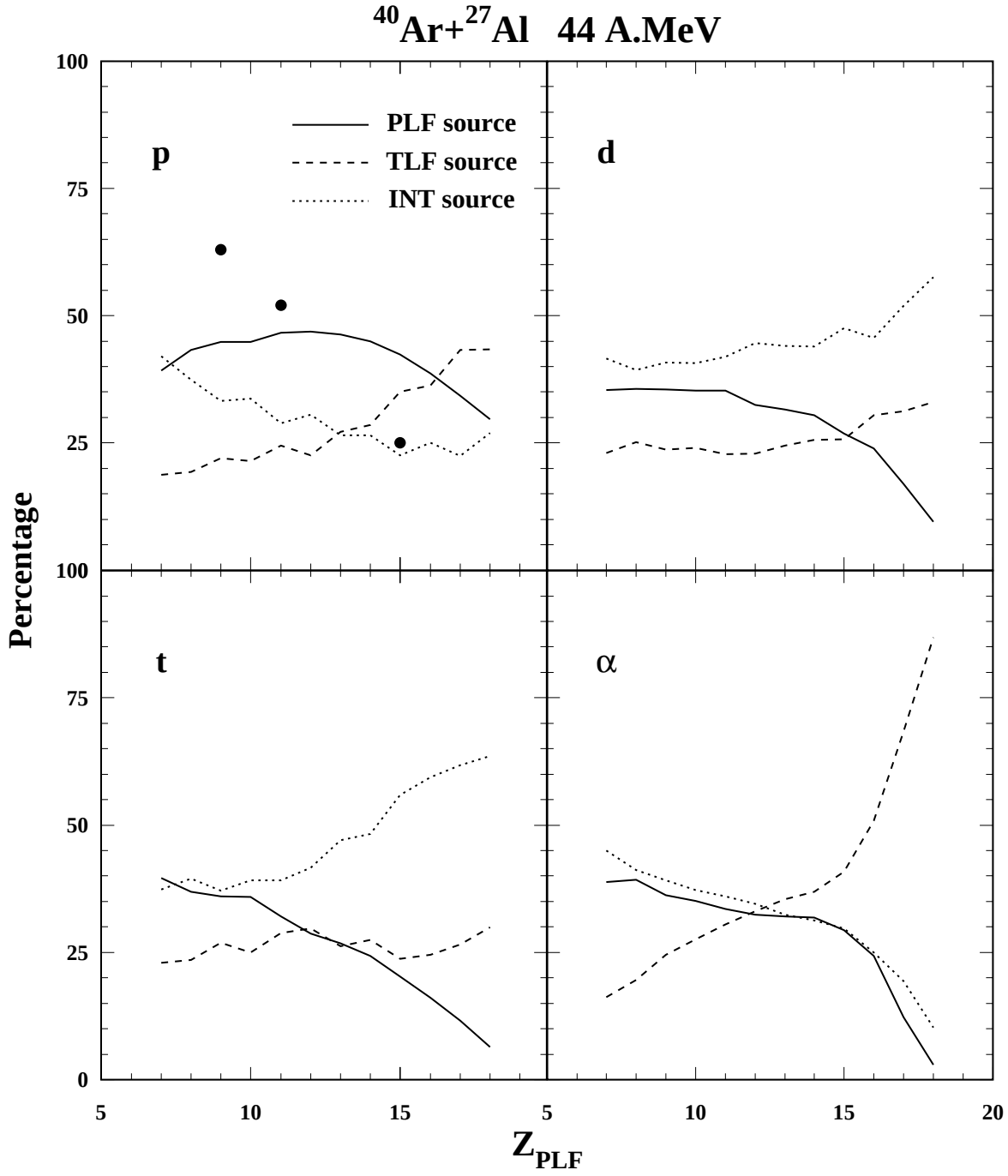
^{40}Ar+^{27}Al 44 A.MeV
PLF source
TLF source
INT source
p
d
t
α
Percentage
Z_{PLF}
100
75
50
25
0
5
10
15
20